TU Delft

Delft University of Technology

Document Version
Final published version

Licence
CC BY

Citation (APA)
de Ridder, M. P., van Kester, D. C. P., van Bentem, R., Teng, D. Y. Y., & van Gent, M. R. A. (2024). Wave overtopping discharges at rubble mound structures in shallow water. *Coastal Engineering*, *194*, Article 104626. https://doi.org/10.1016/j.coastaleng.2024.104626

Important note
To cite this publication, please use the final published version (if applicable).
Please check the document version above.

Copyright
In case the licence states “Dutch Copyright Act (Article 25fa)”, this publication was made available Green Open Access via the TU Delft Institutional Repository pursuant to Dutch Copyright Act (Article 25fa, the Taverne amendment). This provision does not affect copyright ownership.
Unless copyright is transferred by contract or statute, it remains with the copyright holder.

Sharing and reuse
Other than for strictly personal use, it is not permitted to download, forward or distribute the text or part of it, without the consent of the author(s) and/or copyright holder(s), unless the work is under an open content license such as Creative Commons.

Takedown policy
Please contact us and provide details if you believe this document breaches copyrights.
We will remove access to the work immediately and investigate your claim.

This work is downloaded from Delft University of Technology.

Coastal Engineering 194 (2024) 104626

Contents lists available at ScienceDirect

Coastal Engineering

journal homepage: www.elsevier.com/locate/coastaleng

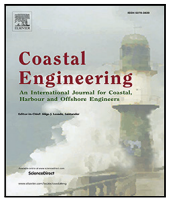

Wave overtopping discharges at rubble mound structures in shallow water

Menno P. de Ridder [a,b,*], Dennis C.P. van Kester [c,b], Rick van Bentem [d], Djimin Y.Y. Teng [a], Marcel R.A. van Gent [a,b]

[a] Deltares, Department of Coastal Structures and Waves, The Netherlands
[b] Delft University of Technology, Department of Hydraulic Engineering, Delft, The Netherlands
[c] Van Oord, Rotterdam, The Netherlands
[d] The Weather Makers,'s-Hertogenbosch, The Netherlands

ARTICLE INFO

Keywords:
Wave overtopping
Shallow foreshore
Rubble mound breakwater
Low-frequency energy
Physical model tests
Empirical expressions

ABSTRACT

Wave overtopping of coastal structures has been studied using physical model experiments with rubble mound breakwaters in shallow water. The mean overtopping discharge is determined for three different foreshore slopes and various hydrodynamic conditions. The hydrodynamic results confirm that energy is transferred to low-frequency waves in very shallow water and that the short waves are in phase with the lower-frequency waves in very shallow water. As a result, the extreme waves (e.g. 2% exceedance wave height) become relatively large in very shallow water due to the energy of the low-frequency waves affecting thereby the wave overtopping. To estimate the amount of energy at the low-frequency waves, an expression is derived which reasonably accurately predicts the low-frequency wave energy (RMSE of 0.06). Considering the non-dimensional overtopping discharge, the existing formulations for the non-dimensional mean wave overtopping discharge perform poorly to reasonably in shallow water with RMSLE ranging from 1.04 to 2.92. A parameter sensitivity study shows that the short-wave steepness, relative crest height and the low-frequency wave height are the most important parameters when predicting the mean overtopping discharge in shallow water. When including the short-wave steepness and relative crest height in an empirical formulation the RMSLE for the current dataset reduces to 0.69. A further increase in accuracy is found when the low-frequency wave height and 2% exceedance wave height are included (RMSLE 0.64).

1. Introduction

The mean wave overtopping discharge is an important parameter for the design and adaption of coastal structures such as rubble mound breakwaters. Adaption of rubble mound breakwaters becomes more important due to climate change because with rising sea levels coastal structures become more exposed to wave attack. An increasing sea level will result in a higher risk of damage to material protected by the structure or flooding of the hinterland. However, it is not trivial to include the effects of climate change, such as sea level rise, in the design of a coastal structure because the climate change scenarios and the sea level predictions contain large amounts of uncertainty. It could therefore be beneficial to apply a climate-adaptive design so that the structure can be changed in the future if the hydrodynamic conditions require it. Such an approach could be more effective, in terms of cost, material and required space, than covering all uncertainty in the initial structure. One of the climate adaptation measures for a rubble mound breakwater is reducing the depth of the foreshore (nourishment) in front of the breakwater to reduce the wave load on the structure (e.g. Van Gent, 2019; Van Gent and Teng, 2023). Such a shallow foreshore can be constructed in front of the breakwater when the current structure no longer meets the safety requirements.

Next to the climate adaptation reason, a shallow foreshore in front of a structure may also be desired to enhance biodiversity. For example, vegetation could be grown on the shallow foreshore, which not only reduces the wave load on the structure (Vuik et al., 2016) but also improves the coastal region's environmental quality (Suedel et al., 2022). Furthermore, a shallow foreshore in front of a coastal structure may also be desirable when requirements are placed on the space or height of the structure. A coastal structure in combination with a shallow foreshore could be preferred when such design restrictions are present because the foreshore will reduce the wave load and thereby the required crest height.

It is known that a shallow foreshore has an effect on the wave loads on a coastal structure (here limited to wave overtopping, see e.g. Van Gent, 1999, 2001; Altomare et al., 2016; Lashley et al., 2021). Various studies have shown that a foreshore can reduce the

* Corresponding author at: Delft University of Technology, Department of Hydraulic Engineering, Delft, The Netherlands.
E-mail address: menno.deridder@deltares.nl (M.P. de Ridder).

https://doi.org/10.1016/j.coastaleng.2024.104626
Received 6 August 2024; Received in revised form 23 September 2024; Accepted 23 September 2024
Available online 27 September 2024
0378-3839/© 2024 The Authors. Published by Elsevier B.V. This is an open access article under the CC BY license (http://creativecommons.org/licenses/by/4.0/).

Nomenclature

α	Structure slope [–]
γ_f	Roughness factor [–]
$\xi_{m-1,0}$	Iribarren number of the structure slope based on H_{m0} and $T_{m-1,0}$ [–] $(\frac{\tan\alpha}{\sqrt{2\pi H_{m0}/(gT_{m-1,0}^2)}})$
η_{LF}	Low-pass band filtered time series of the free surface vertical displacement relative to the SWL [m]
$\langle\eta\rangle$	Wave setup [m]
σ_{LF}	The standard deviation of the low-frequency signal (η_{LF}) [m]
σ_A	The standard deviation of the short-wave group envelope (η_{LF}) [m]
A	Short-wave group envelope [m]
A_s	Wave asymmetry [–]
D_{n50}	Nominal stone diameter (50th quantile of the stone size distribution) [m]
f_p	Peak frequency [Hz]
f_{cutoff}	Cutoff frequency [Hz]
g	Gravitational acceleration [m/s^2]
h	Water depth at the toe of the structure [m]
h_{deep}	The offshore water depth [m]
h_{crest}	Crest level with respect to the flume floor [m]
H_{m0}	Incident significant wave height at the toe of the structure [m]
$H_{m0,deep}$	The offshore incident significant wave height [m]
$H_{m0,LF}$	Incident low-frequency wave height based on a cutoff-frequency at the toe of the structure [m]
$H_{m0,HF}$	Incident high-frequency wave height based on a cutoff-frequency at the toe of the structure [m]
$H_{2\%}$	Incident 2% exceedance wave height at the toe of the structure [m]
k	Wave number associated to $T_{m-1,0}$ and h, through the dispersion relationship [rad/m]
m	Tangent of foreshore slope [–]
q^*	Non-dimensional mean overtopping discharge [–]
q	Mean overtopping discharge [m^3/s/m]
R_c	Crest height above still water level [m]
R^*	Non-dimensional relative crest height [–] (R_c/H_{m0})
$R_{u\%}$	2% exceedance runup level [m]
$R_{A,\eta_{LF}}$	cross-correlation function [–]
$s_{m-1,0,deep}$	Wave steepness based on the offshore $H_{m0,deep}$ and $T_{m-1,0,deep}$ [–] $(2\pi\frac{H_{m0,deep}}{gT_{m-1,0,deep}^2})$
$s_{m-1,0}$	Wave steepness based on the H_{m0} and $T_{m-1,0}$ [–] $(2\pi\frac{H_{m0}}{gT_{m-1,0}^2})$
$s_{m-1,0,HF}$	Short wave steepness based on the $H_{m0,HF}$ and $T_{m-1,0HF}$ [–] $(2\pi\frac{H_{m0}}{gT_{m-1,0}^2})$ $(2\pi\frac{H_{m0,HF}}{gT_{m-1,0,HF}^2})$
S_k	Wave skewness [–]
t	Time [s]
$T_{m-1,0}$	Incident spectral period at the structures toe [s]
$T_{m-1,0,deep}$	Offshore incident spectral period [s]
$T_{m-1,0,HF}$	Incident spectral period of the short waves at the structures toe [s]

wave loads for a dike or a coastal structure. For example, Van Gent (2001) performed physical model experiments with shallow foreshores and assessed the effects of the shallow foreshore on the runup and wave overtopping on dikes and characterized the shallowness of the foreshores by the ratio of the deep water wave height and the local water depth. Lashley et al. (2021) studied the effect of foreshores on the overtopping discharge and found that the mean overtopping discharge reduced exponentially with the ratio of the local water depth over the deep water wave height. To be able to design a coastal structure with a shallow foreshore, the effects of a shallow foreshore should be included in the design methods. Several authors empirically derived a formula for wave overtopping with shallow foreshores (Van Gent, 1999; Altomare et al., 2016; Lashley et al., 2021), but a detailed physical explanation of the effects in shallow water is lacking. Almost all the existing wave overtopping formulations are derived for deep water conditions or derived for dikes and not for rubble mound breakwaters.

Besides the need for an empirical formulation for the mean overtopping discharge to be able to design a rubble mound breakwater including a shallow foreshore, most rubble mound breakwaters are located in shallow water. Thus, not only for climate-adaption or biodiversity a formulation for shallow water is useful, but for the typical rubble mound breakwaters it is also important to have an expression for the mean overtopping discharge including the shallow water processes.

It is not fully understood how shallow water processes affect wave overtopping, but it is known that different processes are important in shallow water in contrast to deep water. Waves start to break and eventually transform into bores for extremely shallow water. As a consequence of depth-limited breaking, the wave height distribution will no longer follow the Rayleigh distribution (e.g. Battjes and Groenendijk, 2000) and the larger waves will become lower. In addition, due to wave breaking the mean water level (wave setup) will increase in the surf zone (Longuet-Higgins and Stewart, 1964). Moreover, due to nonlinear interactions, the wave shape becomes nonlinear resulting in asymmetric waves. Also, energy is transferred from frequencies around the peak of the wave energy density spectrum to lower and higher frequencies. All these processes affect the wave overtopping, but it is yet not fully understood how these effects contribute and how significant their contribution is.

In this study, the effect of a shallow foreshore on the mean overtopping discharge of a rubble mound breakwaters is systematically studied by means of physical model experiments. In Section 2 a literature review is given. The physical model experiments are described in Section 3. The wave propagation over the foreshore is described in Section 4 followed by the results for the mean overtopping discharge in Section 5. The discussion of the results is described in Section 6. Finally, the conclusions are given in Section 7.

2. Background

Wave overtopping has been studied extensively. Saville (1955), Battjes (1972) and Goda et al. (1975) performed physical model experiments related to wave overtopping. One of the first analytical expressions for wave overtopping, which is still the basis of the current formulations, is given by Kikkawa et al. (1968). Their expression is based on the flow over a weir with a simplified oscillating water

level signal, resulting in an exponential function to describe wave overtopping as a function of the crest level.

Owen (1980) performed a series of experiments and derived an empirical exponential formulation for overtopping given by,

$$q^* = a\exp\left(-b\frac{R^*}{\gamma_f}\right) \tag{1}$$

where q^* is the non-dimensional overtopping discharge, R^* the non-dimensional crest level and γ_f a roughness factor. Owen (1980) defined the non-dimensional overtopping as $q/(gH_{m0}T_m)$ and the non-dimensional crest level as R_c/H_{m0}. Several authors have derived similar empirical formulations with different non-dimensional parameters. For example, Franco et al. (1995) used a non-dimensional overtopping discharge given by $q/\sqrt{gH_{m0}^3}$. De Waal and Van der Meer (1993) used the non-dimensional crest level as $(R_{u2\%} - R_c)/H_{m0}$ with $R_{u2\%}$ representing the 2 % runup height. For a complete overview of various formulations and non-dimensional overtopping and non-dimensional crest levels, a reference is made to Hedges et al. (1998).

Battjes (1974) found that the runup height is related to the Iribarren number. Van der Meer and Janssen (1994) extended an overtopping formulation by adding a maximum that does not depend on the Iribarren number. Van Gent (2001) proposed to apply the $T_{m-1,0}$ as a characteristic wave period instead of the mean wave period from the time domain and showed that this wave period can be applied to accurately predict wave runup and wave overtopping for various spectral shapes. Based on these findings the wave overtopping formulation in the TAW (2002) manual is given by,

$$\frac{q}{\sqrt{gH_{m0}^3}} = a\xi_{m-1,0}\exp\left(-b\frac{R_c}{H_{m0}}\frac{1}{\gamma_f\xi_{m-1,0}}\right) \tag{2}$$

with a maximum of

$$\frac{q}{\sqrt{gH_{m0}^3}} = a\exp\left(-b\frac{R_c}{H_{m0}}\frac{1}{\gamma_f}\right) \tag{3}$$

where $\xi_{m-1,0}$ is the Iribarren number given by $\frac{\tan(\alpha)}{\sqrt{s_{m-1,0}}}$ where the wave steepness, $s_{m-1,0}$,is given by $2\pi H_{m0}/(gT_{m-1,0}^2)$. The coefficients a and b were given by 0.067 and 4.74 for Eq. (2) and 0.2 and 2.6 for Eq. (3). Next to an expression for relatively deep water, the TAW (2002) manual provides an expression for shallow or very shallow foreshores based on the work of Van Gent (1999). Van Gent (1999) derived an expression in the range between deep and very shallow water conditions based on physical model experiments with a foreshore slope of 1:100 and 1:250. Based on these results it was concluded that the following expression can be applied to impermeable structures under perpendicular wave attack,

$$\frac{q}{\sqrt{gH_{m0}^3}} = a\exp\left(-\frac{R_c}{H_{m0}\gamma_f(0.33 + 0.022\xi_{m-1,0})}\right) \tag{4}$$

where a is given by 0.12.

Most rubble mound breakwaters have a steep slope making Eq. (3) normative over Eq. (2). Therefore Eq. (3) is provided in EurOtop (2007) for describing the mean wave overtopping discharge for rubble mound breakwaters. In EurOtop (2018) a power was added in the overtopping expression to include applications with a zero to almost zero freeboard,

$$\frac{q}{\sqrt{gH_{m0}^3}} = 0.09\exp\left(-(1.5\frac{R_c}{H_{m0}\gamma_{f,mod}})^{1.3}\right) \tag{5}$$

Note that the addition of the power also affects the influence factors as demonstrated in Van Gent (2022). Next to the addition of the power, the roughness coefficient is changed for very steep and/or very long waves with $\xi_{m-1,0} > 5$,

$$\gamma_{f,mod} = \gamma_f + \frac{(\xi_{m-1,0} - 5)(1 - \gamma_f)}{5} \tag{6}$$

Both Koosheh et al. (2022) and Van Gent et al. (2022) showed that it is important to include the wave steepness in the formulation and derived a formulation with the deep water steepness included. The formulation of Koosheh et al. (2022) is given by,

$$\frac{q}{\sqrt{gH_{m0}^3}} = a\exp\left(-b\left(\frac{R_c}{H_{m0}\gamma_f}\right)^{p_1}s_{m-1,0}^{p_1}\right) \tag{7}$$

with a given by 0.034, b given by 4.97, p_1 given by 1.12 and p_2 given by 0.35. The formulation of Van Gent et al. (2022) is given by,

$$\frac{q}{\sqrt{gH_{m0}^3}} = as_{m-1,0}^{-1}\exp\left(-b\left(\frac{R_c}{H_{m0}\gamma_f}\right)\right) \tag{8}$$

with a given by 0.016 and b given by −2.4. Various studies have added influence factors into these expressions to account for berms, oblique waves, crest walls and roughness elements (e.g. Van Gent, 2014; Chen et al., 2020; Van Gent et al., 2022).

Altomare et al. (2016) also performed experiments with extremely shallow foreshores with a foreshore slope of 1:35 and 1:50. Based on these results they used Eq. (4) by including an equivalent slope ($\tan\delta$) concept in the breaker parameter instead of the actual slope(α) where this equivalent slope is given by,

$$\tan\delta = \frac{1.5H_{m0} + R_{u2\%}}{(1.5H_{m0} - h)\cot m + (h + R_{u2\%})\cot\alpha} \tag{9}$$

where m is the foreshore slope and $R_{u2\%}$ is the wave run-up level exceeded by 2% of the incident waves given by,

$$\frac{R_{u2\%}}{H_{m0}} = \left(4 - \frac{1.5}{\sqrt{\xi_{m-1,0}}}\right) \tag{10}$$

In this definition, the breaker parameter is related to the $R_{u2\%}$, but this parameter is also related to the breaker parameter. This means that the solution has to be found with an iterative method.

Lashley et al. (2021) suggested another approach with a formulation based on deep water conditions. The effect of the foreshore is included in the formulation for the mean overtopping discharge. This formulation is thus given in terms of deep water conditions and it is given by,

$$\frac{q}{\sqrt{gH_{m0}^3}} = a\exp\left(-b\frac{R_c}{H_{m0,deep}} + c\frac{h}{H_{m0,deep}}\right) \tag{11}$$

where h is the water depth at the toe and $H_{m0,deep}$ the deep water wave height. The coefficients a, b and c are a function of the deep water wave steepness and the foreshore slope. Depending on the relative water depth ($h/H_{m0,deep}$) three regimes were defined for which each regime had its own formulation for a, b and c. One drawback of this approach is that the processes over the foreshore are indirectly taken into account in the expression. This means that the formulation does not take into account the processes happening at the foreshore. For example, a foreshore with and without a breaker bar results in the same mean overtopping discharge with such an approach, whereas the dynamics of the waves at the toe of the structure could be different.

The importance of wave breaking on the shallow foreshore was characterized by Van Gent (1999) with the ratio of the deep water wave height over the local water depth. This ratio indicates the intensity of wave breaking and the potential importance of low-frequency waves. For $H_{m0,deep}/h$ smaller than 0.4 the conditions can be characterized as 'deep' meaning that limited wave breaking occurs and limited energy is transferred to lower frequencies; for $H_{m0,deep}/h$ between 0.4 and 1 the conditions can be characterized as 'intermediate' with wave breaking occurring and transfer of energy to low frequencies; for $H_{m0,deep}/h$ between 1 and 3 the conditions can be characterized as 'shallow' with severe wave breaking and severe energy in the lower frequencies; and for $H_{m0,deep}/h$ larger than 3 the conditions can be characterized as 'very shallow' where the short waves do hardly contain energy because all energy has been dissipated or transferred to lower-frequencies.

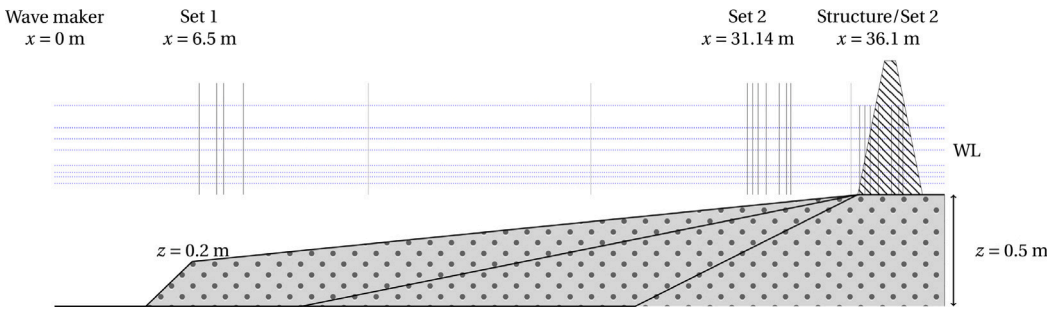

Fig. 1. Schematic overview of model Layout A, B and C. Wave gauges as part of a set are shown in black. The gray instruments represent wave gauges that are not part of a set. Note that the scale is distorted to visualize the layout. The position of wave gauge Set 2 is shown both at the location and during the calibration tests and the test with the breakwater.

3. Wave flume tests

3.1. Model set-up

Physical model experiments were conducted in a wave flume (Scheldt Flume at Deltares, Delft). Waves were generated with a piston wave maker including second-order waves and reflection compensation. This means that the reflections from the structure are absorbed at the wave board and that the spurious waves are minimized by generating the second-order waves.

A concrete foreshore with a slope of 1/100 (A series), 1/50 (B series) and 1/20 (C series) with a height of 0.5 m was constructed in the wave flume with a rubble mound breakwater at the end of the foreshore (see Table 1 and Fig. 1). A step of 0.2 m is applied at the start of the foreshore for the tests with a 1/100 slope because the flume is too short to fit the entire 1:100 slope. This step will affect the hydrodynamics (Eldrup and Lykke Andersen, 2024), but it is argued that the effect is limited because the transition is in relatively deep water and positioned relatively far away from the toe of the structure. The three foreshore slopes were mainly required to obtain different wave conditions for the same water depth at the toe of the structure (see Fig. 1).

The rubble mound breakwater has a similar geometry for all the tests with a slope of 1/2 (see Fig. 3). The structure consists of a core with a D_{n50} of 8.5 mm and an armour layer with a D_{n50} of 23.9 mm. This means that the porosity of the armour layer is approximately 0.4. When following the TAW (2002) guidelines or the EurOtop (2018) guidelines this results in a roughness factor of 0.55 or 0.40 for applications of Eq. (2) and Eq. (3), or Eq. (5) respectively (Rocks 2 layers, permeable core). The stones were fixed with epoxy glue such that they did not move during the tests. The flume was split into two parts at the location of the structure (see also Panel D of Fig. 2). One side was used to measure the water layer thickness with the relative long crest element of 0.5 m (height of 50 mm). On the other side, the crest element was shorter and an overtopping chute was placed at the end of the structure to capture the overtopping volumes into an overtopping box. In this way both the spatial effects of the water layer thickness can be studied with the side with the long crest element (not used in this study) and the mean overtopping discharge can be measured with the side with the shorter crest element, although water layer thicknesses are not part of the analysis here. All experiments were also conducted without the structure (calibration tests) and a wave absorber at the end of the flume to obtain the incident wave condition at the location of the breakwater. During the calibration tests, Set two of wave gauges was moved to the position of the structure (the horizontal part behind the sloping foreshore, $x = 36.18$ m).

Various water levels were tested to obtain results for both relatively deep and shallow conditions. The offshore water depth varied between 0.55 m and 0.9 m. For every water level variation, the crest level was varied to obtain overtopping discharges in the same range for all the tests.

Two sets of wave gauges were applied to measure the free surface elevation. A set at deep water with four wave gauges and a set of seven wave gauges at the foreshore in case of the tests with the breakwater or located at the horizontal part in case of the calibration test. In addition to these two sets, three additional wave gauges were placed at the foreshore. An overtopping box with two wave gauges was applied to measure the overtopping volume.

3.2. Incident waves

The incident waves at the toe were obtained from the first wave gauge from wave gauge Set Two during the calibration tests. This means that the incident wave conditions are obtained at the location of the structure. Since the incident wave signals are obtained from the calibration tests without the structure in place, the effect of the reflection on the incident wave signal is not included. It is argued that the signal without the effect of the reflection is more useful for design purposes because the hydrodynamic conditions during the design phase are mostly obtained from a numerical wave model which also does not include the reflections from the structure.

Because the waves become very nonlinear and transform into breaking rollers for shallow water conditions, the measured high-passed free surface signal during the calibration tests is applied as an incident wave signal instead of a signal from a decomposition method. It is observed that the decomposition method does not capture the very nonlinear wave shape in very shallow water. The assumption that the high-passed free surface signal represents the incident wave signal is valid because the reflection of the short waves at the wave absorber is very small. This does not hold for the long waves, where significant reflections (20%) were observed during the calibration tests. Therefore, the nonlinear wave decomposition method described in De Ridder et al. (2023) is applied for the low-passed free surface elevation with a cutoff frequency equal to the peak frequency divided by two.

Based on the incident wave signal measured at the toe of the structure during the calibration tests the incident wave parameters are computed. The spectral parameters significant wave height (H_{m0}) and spectral period ($T_{m-1,0}$) are computed based on the spectral moment $m_n = \int_{\Delta f}^{f_{max}} f^n E(f) df$. The spectral wave parameters are computed for the entire frequency range from 0 to f_{max}. To distinguish between the short and long waves, both the wave height and spectral period are also computed for the high and low frequency of part of the spectrum based on a cutoff frequency. The low-frequency wave parameters (indicated as LF) are computed based on the frequency range between 0 and f_{cutoff}. The high frequency parameters (indicated as HF) are computed based on the frequency range between f_{cutoff} and f_{max}. The sensitivity of the results to this cutoff frequency is shown in Section 5.5 with optimal results in terms of mean overtopping predictions for a cutoff frequency of $f_p/1.5$. Note that this cutoff frequency is different than applied for the wave separation, but also has a different purpose. Besides the definition, also a practical effect is considered. For the current

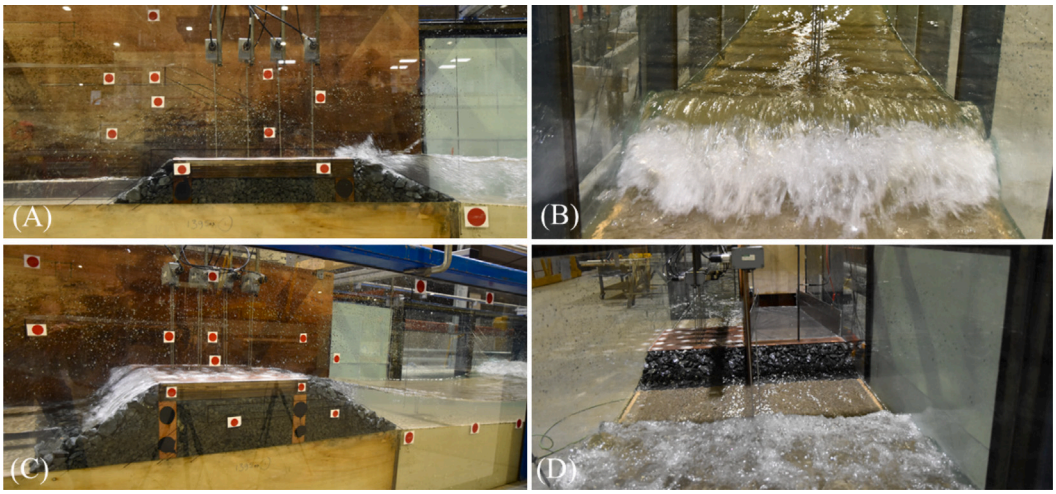

Fig. 2. Photos of the model setup. Panel A shows the rubble mound breakwater with a structure height of 0.05 m (incident waves from right to left). Panel B shows the severe wave breaking in front of the rubble mound breakwater. Panel C shows an overtopping event for a structure with a structure height of 0.22 m. The separation of the flume into two parts is shown in Panel D.

Table 1
Locations of wave gauges and position of foreshore. The location of the wave gauges shown in this table is representative of the tests with the structure in place. During the calibration tests wave gauge Set two is moved to $x = 36.18$ m. The location of the wave gauges during the calibration test are indicated as Calibration set-2. The bed levels for Wave gauges five, six and seven are shown for respectively Series A, B and C. For the other wave gauges the bed levels are not shown.

Feature	Location w.r.t wave board [m]	bed level [m]
Wave board	0.00	0.00
Start step (1/100)	4.18	0.00
End step (1/100)	6.18	0.20
Start foreshore 1/100	6.18	0.2
WHM01 (set-1)	6.50	–
WHM02 (set-1)	7.28	–
WHM03 (set-1)	7.59	–
WHM04 (set-1)	8.48	–
WHM05	14.10	0.28/0.06/0.00
WHM06	24.10	0.38/0.26/0.00
WHM07	35.80	0.50/0.50/0.49
WHM08 (set-2)	31.14	–
WHM09 (set-2)	31.38	–
WHM10 (set-2)	31.72	–
WHM11 (set-2)	31.98	–
WHM12 (set-2)	32.57	–
WHM13 (set-2)	32.90	–
WHM14 (set-2)	33.09	–
End foreshore	36.18	0.5
WHM08 (Calibration set-2)	36.18	–
WHM09 (Calibration set-2)	36.42	–
WHM10 (Calibration set-2)	36.66	–
WHM11 (Calibration set-2)	37.02	–
WHM12 (Calibration set-2)	37.61	–
WHM13 (Calibration set-2)	37.94	–
WHM14 (Calibration set-2)	38.13	–
Start structure	36.18	0.50
Wave damper (1/100 and 1/50)	43.18	0.50
Wave damper (1/20)	40.13	0.50

tests, it was possible to define the cutoff frequency based on the peak frequency, but this is in reality not easy because the wave spectrum shape could be more complicated than a single-peaked spectrum with a clear peak frequency. Therefore, it is suggested to determine the cutoff frequency based on the offshore spectral period. This results in a cutoff frequency of $f_{cutoff} = 0.45/T_{m-1,0}$. This definition is verified for the current findings and also shows accurate results. Therefore, this definition is recommended to apply in practical cases. In the effects of these choices on the measured wave parameter are demonstrated. Next to the spectral parameters, the exceedance curves are computed and the 2% exceedance wave height ($H_{2\%}$) is used hereafter. Due to the significant wave energy of the long waves in shallow water, the individual waves are determined with a crossing of the time series with a low-frequency signal. The wave setup, $\langle\eta\rangle$, is determined as the deviation between the still water level before the test and the mean signal after 5 min. In the analysis, the first 90 s are not included in the time series to determine the wave parameters because the wave field and mean water levels are not stationary just after the test starts.

3.3. Test programme

The test programme consists of variations in the wave height ($H_{m0,deep}$), deep water wave steepness ($s_{m-1,0,deep}$), crest height (R_c) and water depth (h_{deep}). These variations are applied for three different foreshore slopes (see Table 2). Not all crest height and water level combinations were tested because not all combinations result in significant

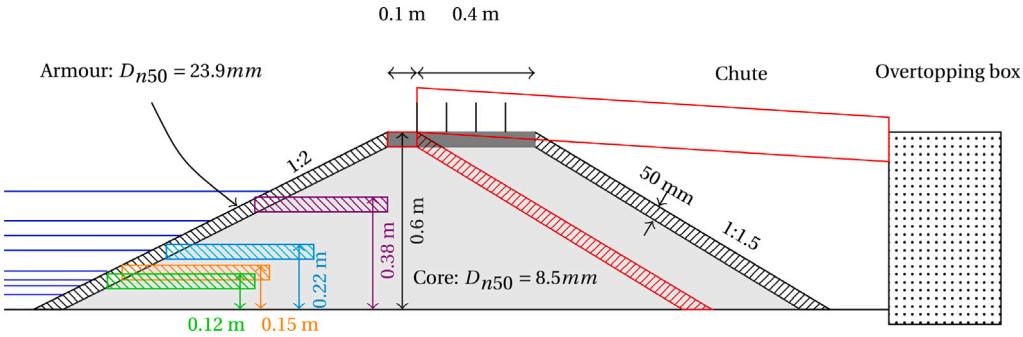

Fig. 3. Cross section of the rubble mound breakwaters. The geometry in red shows the side with the overtopping box and the geometry shown in black is at the side with the longer crest element to measure the water layer thickness. The crest levels of the various configurations are shown in colours (green, orange, cyan, violet and black). The tested water levels are shown in blue.

Table 2
Variations applied in the physical model experiments. Water depth (h_{deep}) and crest height (h_{crest}) are defined with respect to the bottom of the wave flume.

Parameter	Symbol	Variation
Wave height	H_{m0} [m]	0.1, 0.15, 0.2 and 0.25
Deep water wave steepness	$s_{m-1,0}$ [–]	0.015, 0.025 and 0.04
Foreshore slope	m [–]	1/100, 1/50 and 1/20
Configurations (Offshore water depth and crest level)	h_{deep} and h_{crest} [m]	4: $h_{deep} = 0.90$, $h_{crest} = 1.1$ 5: $h_{deep} = 0.80$, $h_{crest} = 1.1$, 3: $h_{deep} = 0.70$, $h_{crest} = 0.88$, 6: $h_{deep} = 0.75$, $h_{crest} = 0.88$ 2: $h_{deep} = 0.60$, $h_{crest} = 0.72$ 7: $h_{deep} = 0.63$, $h_{crest} = 0.72$ 1: $h_{deep} = 0.55$, $h_{crest} = 0.65$ 8: $h_{deep} = 0.58$, $h_{crest} = 0.65$ 9: $h_{deep} = 0.55$, $h_{crest} = 0.62$

wave overtopping. In Table 2 the nine combinations are shown (each combination is indicated with a testID). Moreover, not the same tests executed with the 1/100 slope are repeated with the 1/20 and 1/50 foreshore slope because the main interest is to obtain shallow water conditions at the toe of the structure and the deeper water conditions for the 1/20 or 1/50 slope would not deviate much from the conditions obtained with the 1/100 foreshore slope. All tests were repeated with the same steering conditions but without the structure to obtain the incident waves (calibration test). The wave signal at the wave maker consists of random waves from a JONSWAP spectrum with a duration of approximately 1000 waves.

In total 144 tests were performed (excluding the calibration tests). 24 tests with a 1:20 foreshore, 39 tests with a 1:50 foreshore and 81 with a 1:100 foreshore. In Table 3 an overview is given of all the (incident) parameter ranges in the dataset at the toe of the structure. Due to variations in both the wave steepness and foreshore slope, various type of breakers (spilling, plunging and surging) are present in the dataset (see also Fig. 2).

3.4. Error metrics

The error metric used in this study is the root-mean-square-error (RMSE) or root-mean-square-logarithmic-error (RMSLE). The definition of the RMSE and RMSLE are given by Eqs. (12) and (13),

$$RMSE = \sqrt{\left(\frac{1}{N}\sum_{i=1}^{N}(x_i - y_i)^2\right)} \tag{12}$$

$$RMSLE = \sqrt{\left(\frac{1}{N}\sum_{i=1}^{N}(\log(x_i + 1) - \log(y_i + 1))^2\right)} \tag{13}$$

where x_i is the modelled value, y_i the observed value and N the number of values. To show the accuracy of the existing formulation the scatter index and relative bias are also considered which are given by,

$$SCI = \frac{\sqrt{\langle((\langle x\rangle - \langle x\rangle) - (\langle y\rangle - \langle y\rangle))^2\rangle}}{\langle y\rangle} \tag{14}$$

$$\text{Rel. bias} = \frac{\sum_{i=1}^{N}(x_i - y_i)}{\sum_{i=1}^{N}(y_i)} \tag{15}$$

where $\langle ... \rangle$ is the mean operator.

4. Wave propagation over the foreshore

This section shows the hydrodynamic results at the location of the structure related to the shallow water processes. Due to the shallow water depth at the foreshore, different processes are important to describe the wave field. Both wave breaking, wave setup, low-frequency waves and the wave shape are considered.

4.1. Wave breaking

For the shallow water tests, the wave height at the foreshore is lower than generated with the wave maker. Due to depth-limited wave breaking, energy is dissipated over the foreshore. In Fig. 4 the wave height at the foreshore as a fraction of the deep water wave height is shown for different local water depths normalized with the deep water wave height. The colours of the points show the deep water wave steepness. The limits of the deep ($H_{m0,deep}/h < 0.4$), intermediate ($0.4 < H_{m0,deep}/h < 1$), shallow ($1 < H_{m0,deep}/h < 3$) and very shallow ($H_{m0,deep}/h > 3$) are shown as black vertical lines. For relatively shallow conditions ($h/H_{m0,deep} \approx 0.33-1$), the wave height is significantly lower than the deep water wave height. In most of the tests, the results follow the same relation, but only tests with a 1:20 slope deviate from this line (square markers). The wave height in the 1:20 series is slightly

Table 3
Parameters range of test programme. The incident wave parameters are obtained from wave gauge Set two (toe of the structure).

Parameter	Symbol	Values/Ranges
Seaward slope (–)	$\cot\alpha$	2
Armour stone diameter (m)	D_{n50}	0.023
Water depth (m)	h	0.05–0.4
Incident wave height (m)	H_{m0}	0.03–0.21
Incident low-frequency wave height (m)	$H_{m0,LF}$	0.01–0.06
Wave steepness (–)	$s_{m-1,0}$	0.001–0.040
Short-wave steepness (–)	$s_{m-1,0,HF}$	0.004–0.047
Iribarren number (–)	$\xi_{m-1,0}$	0.05–1.11
Freeboard (m)	R_c	0.12–0.6
Foreshore slope (–)	m	1/100,1/50,1/20
Non-dimensional freeboard (–)	R_c/H_{m0}	0.80–3.72
Non-dimensional stone diameter (–)	D_{n50}/H_{m0}	0.12–0.89
Relative low-frequency wave height (–)	$H_{m0,LF}/H_{m0}$	0.10–0.81
Relative water depth (–)	h/H_{m0}	0.57–4.95

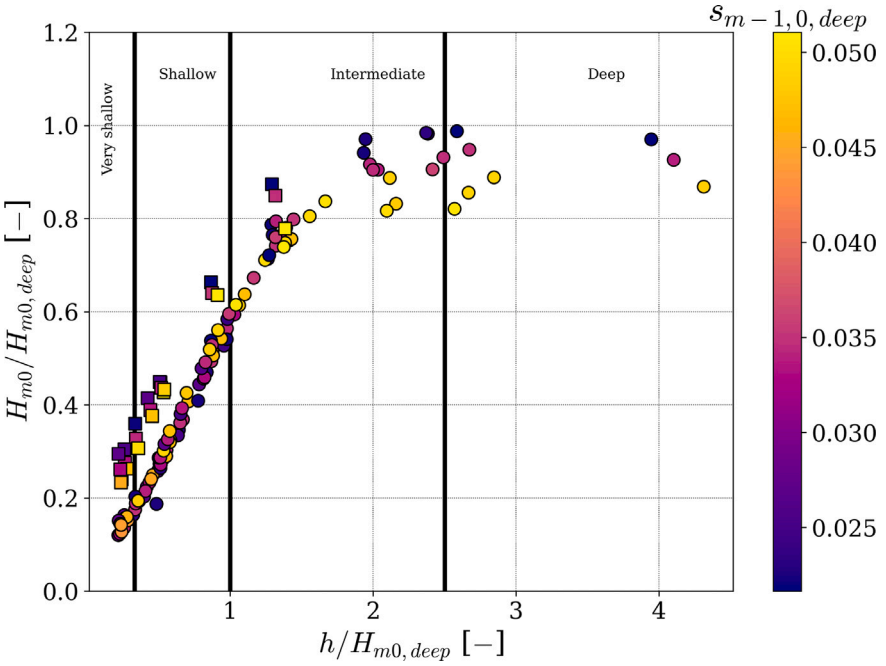

Fig. 4. Foreshore wave heights over deep water wave heights as a function of the local water depth divided by the deep water wave height. The colours indicate the deep water wave steepness. The black vertical lines show the limits of the regions: deep, intermediate, shallow and very shallow. The wave conditions with a foreshore slope of 1/100 and 1/50 are shown with a circle and the 1/20 wave conditions are shown with a square.

higher than observed in the 1:50 and 1:100 series because shoaling is more pronounced and the surf zone is shorter. This means that the wave energy at the end of the foreshore is larger than for the other two foreshores. But in general, it is observed that all foreshore slopes do show a significant reduction of wave energy up to 85%. In deeper water ($H_{m0,deep}/h < 0.4$), the wave steepness is affecting the dissipation of wave energy. The low steepness condition contains more energy compared to the high wave steepness condition. For these deep water conditions, the wave breaks based on the steepness of the waves.

4.1.1. Wave height distribution

Besides, the reduction of the wave height, it is known that the wave height distribution will also change in shallow waters (see for instance Battjes and Groenendijk, 2000). Due to wave breaking the largest waves start to the break first meaning that the distribution does not follow a (deep water) Rayleigh distribution. This behaviour is also visible in the current dataset. The conditions with a relatively deep water depth show a distribution similar to a Rayleigh distribution, but as the water depth decreases the wave height in the tail becomes lower. For a Rayleigh distributed wave field the ratio between the $H_{2\%}$ and the H_{m0} is 1.4. In Fig. 5 this ratio is shown as a function of the energy at the low-frequency wave height. The colours of the points show the relative water depth. To distinguish between the short and long waves the energy of the short waves is used as characteristic wave height.

This figure shows that when waves propagate from deep to shallower water ($H_{m0,deep}/h \approx 0.7$), the 2% exceedance wave height reduces due to wave breaking. This corresponds to an increase in the low-frequency energy fraction from 0.1 to 0.3. The exceedance distribution will no longer follow the Rayleigh distribution for these water depths. When the water depth further decreases and relatively more energy is present at the lower frequencies ($H_{m0,LF}/H_{m0} > 0.3$), the ratio between the 2% exceedance wave height and short-wave height increases again. Due to the energy at the low-frequency waves, the short waves are present at a higher level resulting in a larger 2% exceedance wave height compared to the situation without much energy at the lower frequencies. For extremely shallow water the 2% exceedance wave height is much larger than in a Rayleigh distributed wave field. This behaviour is relevant because the 2% exceedance wave height is a characteristic parameter to describe the highest waves that lead to wave overtopping. Thus, both the effect of breaking as the energy transfer to the lower frequencies are included in this parameter.

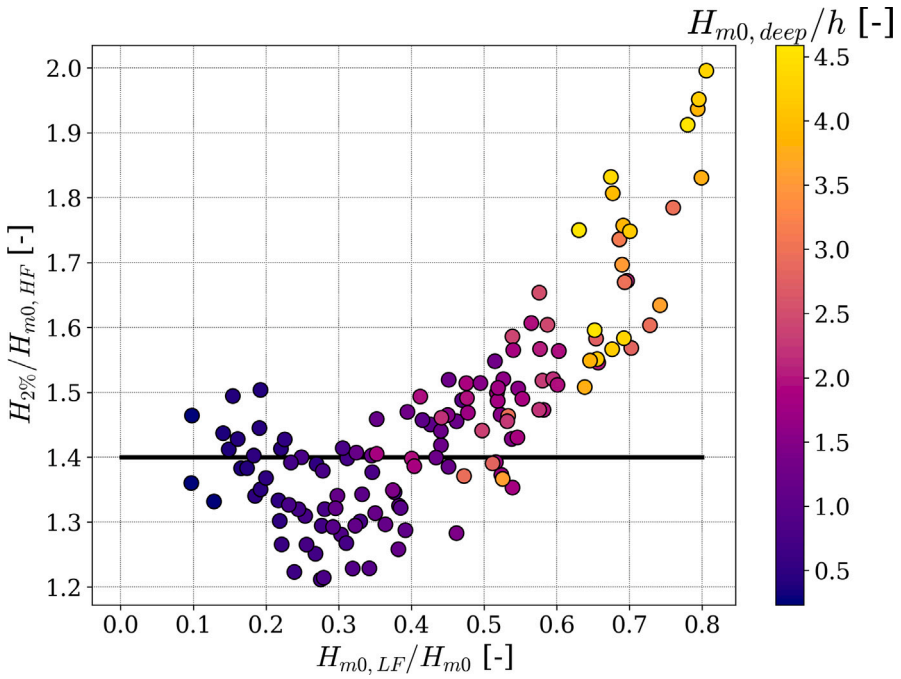

Fig. 5. Ratio between the 2% exceedance wave height ($H_{2\%}$) and the short-wave height ($H_{m0,HF}$) as a function of the relative low-frequency wave height ($H_{m0,LF}/H_{m0}$). The colours indicate the relative water depth. The deep water relation for Rayleigh distributed waves is shown as a horizontal black line.

4.1.2. Wave setup

Due to the wave breaking the mean water level in front of the structure, the wave setup, will be larger than the still water level. In Fig. 6 the wave setup divided by the water depth is plotted against the relative water depth. This result shows that the wave setup is negligible in deep water where the wave setup is less than 2% of the water depth. But in shallow water, the setup increases up to 20% of the water depth. Also note that a negative setdown is observed before a relative depth of 1. The magnitude of the setup is related to the offshore wave height and local water depth. For a larger wave height or lower water depth, the setup increases. The same results are found for the 1:100 and 1:50 foreshore slopes, but the 1:20 slope deviates. In water depths $H_{m0,deep}/h$ between 1 and 3 the setup is lower than for the 1:100 and 1:50 tests. This deviation could be explained by the fact that the breaking process is different for this steep slope. The breaking zone is much shorter for the 1:20 foreshore slope. For a very shallow foreshore ($H_{m0,deep}/h > 3$) severe wave breaking occurs irrespective of the foreshore slope and the wave set-up does not depend on the foreshore slope.

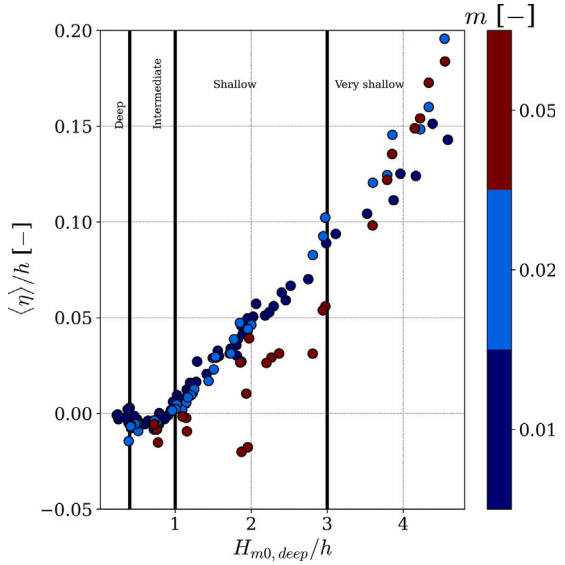

Fig. 6. Non-dimensional wave setup as a function of the relative water depth. The foreshore slope is shown with the marker colour. The results are obtained from Wave gauge WHM07 (in front of the structure). The black vertical lines show the limits of the regions: deep, intermediate, shallow and very shallow.

4.2. Nonlinear wave interaction

When waves propagate into shallow water, energy from the primary waves is transferred to higher and lower frequencies (Longuet-Higgins and Stewart, 1962; Hasselmann, 1962). The transfer of energy within the spectrum is shown in Fig. 7 for Test A912 (1 : 100 foreshore, $H_{m0,deep}/h = 2$, $s_{m-1,0,deep} = 0.01$). For various relative water depths in the wave flume, the wave spectrum is shown. When the water depth becomes shallower, waves start to break and the energy at the peak and the higher harmonics dissipate, but the energy at the lower frequencies is still increasing. Due to the very long wavelength of these low-frequency waves, these long waves do not break. Only the 1/100 foreshore breaking of the low-frequency waves is observed. This large amount of energy at the low frequencies explains why large wave heights can be observed in shallow water. When considering the time series, it is observed that in relatively deep water ($H_{m0}/h < 0.78$) the low-frequency time series is out of phase with the wave group as found by several authors (Battjes et al., 2004; Janssen et al., 2003). This behaviour is quantified with the cross-correlation function ($R_{A,\eta_{LF}}$) between the low-frequency signal (η_{LF}) and the short-wave group envelope (A) defined as,

$$R_{A,\eta_{LF}}(\tau = 0) = \frac{\langle \eta_{LF}(t) \rangle \langle\, A(t+\tau) \rangle}{\sigma_{LF}\sigma_A} \tag{16}$$

where σ_{LF} is the standard deviation of the low-frequency signal and σ_A is the standard deviation of the short-wave group envelope. The short-wave group envelope is based on the absolute value of the Hilbert transform of the signal (See also Janssen et al., 2003). Only the cross-correlation function for a time shift of zero ($\tau = 0$) is considered in this section assuming that there is no phase lag.

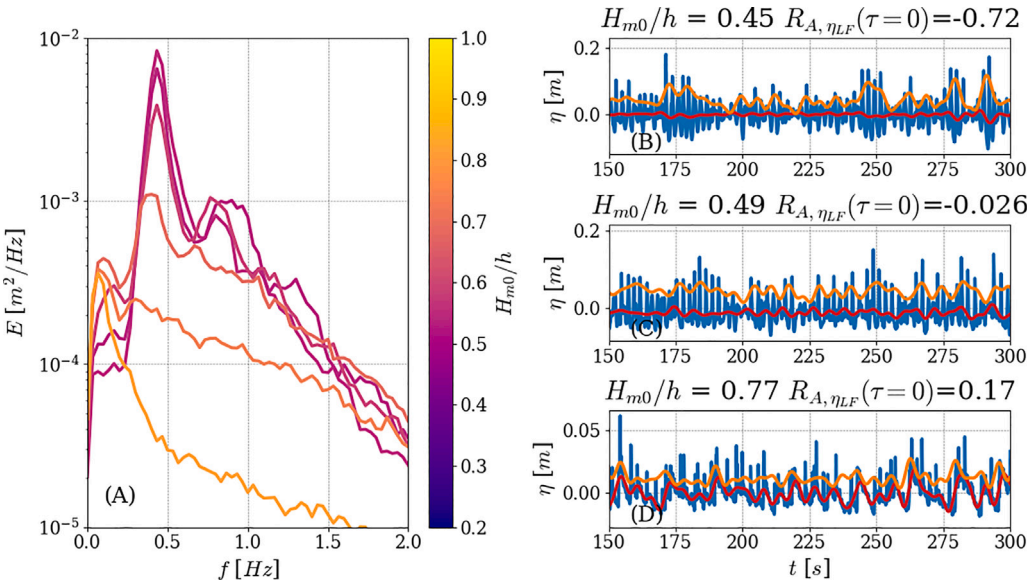

Fig. 7. Wave spectrum at various locations in the wave flume for a test with 1 : 100 foreshore, $H_{m0,deep}/h = 2$, $s_{m-1,0,deep} = 0.01$ (Panel A). For three locations (Panels B, C and D), the time series of the total observed signal (blue), the low passed signal (red) and the wave envelope (orange) are shown.

In deep water the cross-correlation function is negative (meaning that the low-frequency wave signal is out of phase with the short-wave group). However, in shallow water, the cross-correlation function becomes positive (meaning that the low-frequency wave signal is in phase with the short-wave group). Due to wave breaking the low-frequency waves become free and the short waves can only exist on the crest of a low-frequency wave because the water depth below the crest is higher than below the trough. Thus, the low-frequency waves carry the short waves in shallow water. In Fig. 7 this is shown with a $R_{A,\eta_{LF}}$ of −0.72 in relatively deep water and a $R_{A,\eta_{LF}}$ of 0.17 in shallow water.

For every test the cross-correlation function for a zero phase shift ($\tau = 0$) is determined for several locations in wave flume (WHM01, WHM04, WHM05, WHM06, WHM07 and WHM08) during the calibration tests (see Fig. 8). This analysis shows that in deep water the cross-correlation function is negative. When the relative water depth decreases the cross-correlation function becomes more negative showing that the correlation becomes higher. This can be explained by more energy at the low-frequency wave. From a relative water depth of 2, the cross-correlation function increases again and at a relative depth of 1 becomes positive. Thus, for these conditions, the low-frequency wave is in phase with the short-wave group which means that the higher short waves propagate over the crest of low-frequency waves.

Next to the sign of the cross-correlation function, the time shift (τ) for the maximum correlation also changes when the water depth decreases. When the low-frequency wave shoals it starts to lack behind the short-wave group resulting in a maximum correlation at a non-zero time shift (See also Janssen et al., 2003). In Appendix B this is illustrated by showing the cross-correlation function for different time shifts which shows that the time shift for the maximum correlation becomes longer when the water depth decreases. This will also affect the magnitude of the cross-correlation function with a zero time shift. When only considering the cross-correlation function with zero time shift (as done in Fig. 8), the magnitude of the correlation becomes smaller when the maximum correlation shifts. This explains why the correlation increases for a relative water depth between 1 and 2.

4.3. Expression for the low-frequency wave height

In Fig. 9 the energy at the lower frequency divided by the total wave energy is shown as a function of the kh where h is the water depth at the location of the structure and k the wave number computed with the dispersion relation with the deep water spectral period ($k = \mathrm{disp}(1/T_{m-1,0}, h)$). In deep water ($kh > 1$), the energy of these low-frequency waves is relatively low and contributes to 10%–15% of the total wave energy. However, in more shallow water the contribution of the low-frequency waves becomes much larger. In very shallow water ($kh \approx 0.25$) the wave height is for more than 70% given by the low-frequency waves. Almost all the wave energy is present at a different time scale than forced at the wave maker. The fraction between the energy at the lower frequencies and the total energy can be related to kh reasonably well. Next to the kh the wave steepness also shows an effect on the fraction of low-frequency energy. The wave conditions with a larger wave steepness have relatively more energy at the lower frequencies for the same kh. Note that the kh also depends on the wave period. In general, the tests with a lower wave steepness do have more energy at the lower frequencies, but when correcting for the kh, the wave steepness also shows an influence.

When the energy of the lower frequencies is quantified with an empirical expression, the fraction of low-frequency wave energy can reasonably accurately be determined (see Table 4). An expression with both the deep water wave steepness and kh results in an RMSE of 0.071. When this formulation is fitted for a subset of the dataset based on the foreshore slope, it is observed that the factor in front of the formulation changes slightly. The tests with a steeper foreshore result in less low-frequency energy compared to tests with a milder slope as also found in earlier studies (e.g. Battjes et al., 2004). When the foreshore slope is included the RMSE reduces to 0.060 (Eq. (21)). Compared to a similar expression given in Van Gent and Giarrusso (2005) the current formulation improves the accuracy (RMSE of 0.27 for expression in Van Gent and Giarrusso, 2005).

These findings are valid for straight foreshore slopes with long-crested waves. It is known that the short-crested sea states will result in a lower amount of low-frequency energy (Klopman and Dingemans, 2001, e.g.). Moreover, complex bathymetries could result in different behaviour. In the current setup the low-frequency waves shoal as bound waves to the short-wave groups whereas, for instance, on a foreshore with a breaker bar, the short waves could break over the breaker bar resulting in free low-frequency waves. This could result in a different fraction of low-frequency energy because free waves shoal different than bound waves. Thus, due to short waves propagating on the crest of low-frequency waves in shallow water, the short waves at the structure

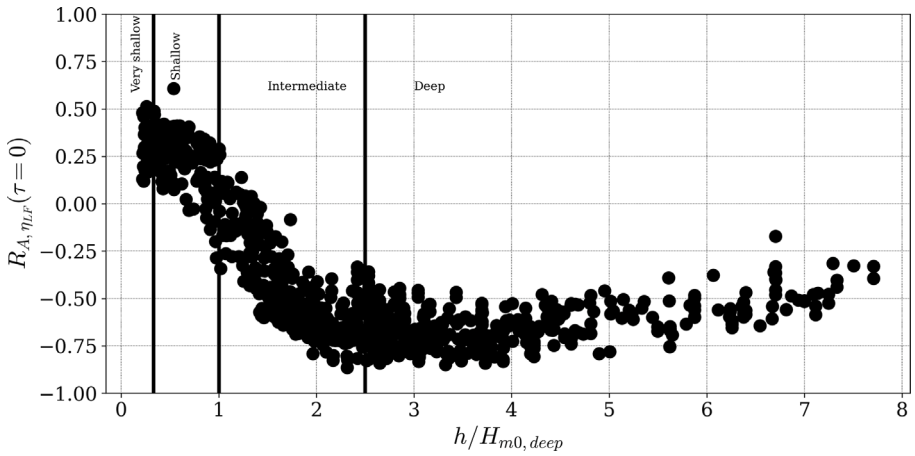

Fig. 8. Cross-correlation function between low-frequency signal (η_{LF}) and short-wave group (A) as a function of the relative water depth expressed in the deep water wave height ($h/H_{m0,deep}$). The results are obtained from signals at Wave gauges WHM01, WHM04, WHM05, WHM06, WHM07 and WHM08. The black vertical lines show the limits of the regions: deep, intermediate, shallow and very shallow.

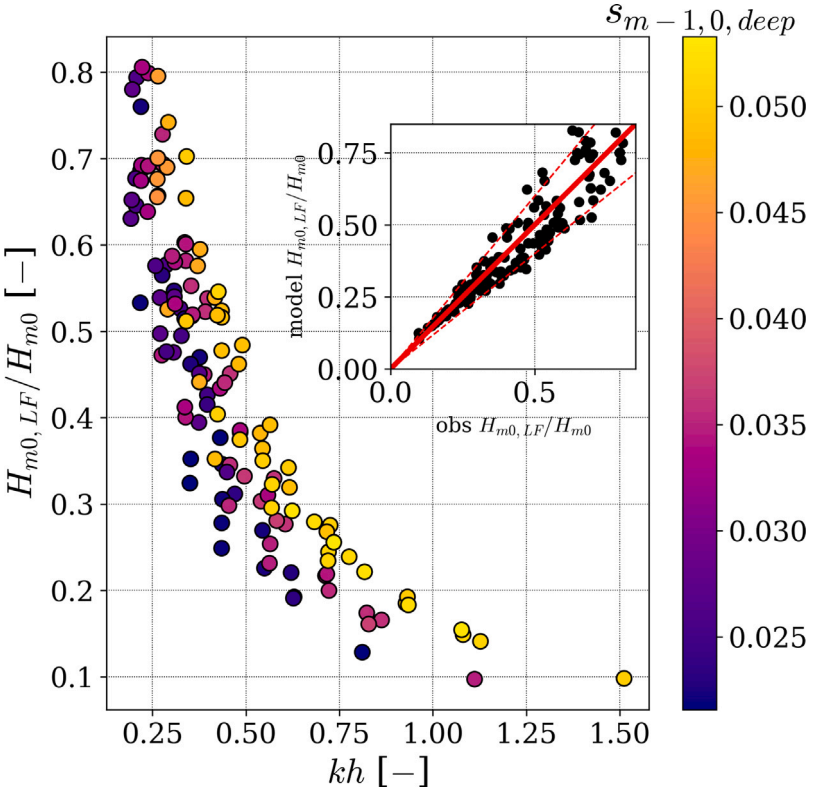

Fig. 9. Low-frequency wave energy divided by the total wave energy as a function of the kh The wave steepness of the waves at deep water is indicated with a colour. The scatter plot shows the performance of Eq. (21).

can become relatively large. The amount of low-frequency energy can be estimated with an empirical expression (Table 4), which can be used for predicting wave overtopping discharges.

5. Overtopping results

For each test, the mean wave overtopping discharge is determined based on the total volume in the overtopping box divided by the duration of the test. The results for the very low non-dimensional mean overtopping discharges ($q/\sqrt{gH_{m0}^3} < 10^{-6}$) are not considered to be reliable because these results could be affected by scale effects. The values of these low mean overtopping discharges are shown in all the figures but are not applied in the computations of the statistics since the reliability of low discharges reduces for lower discharges due to scale effects. The performance of the formulations is evaluated with the RMSLE of the non-dimensional overtopping discharge as error metric (see Section 3.4).

5.1. Comparison with existing formulations

When the results are compared to the existing formulations, significant deviations are found (see Fig. 10). The roughness factor as used when deriving the formulation is applied because the formulations are very sensitive to the applied roughness factor. This results in a γ_f (double layer armour) of 0.55 (as proposed for rock by TAW, 2002) for Van Gent (1999), TAW (2002) and Koosheh et al. (2022) and

Table 4
Ratio of low-frequency wave height and the total incident wave height.

Formulation		m [–]	RMSE [–] ($H_{m0,LF}/H_{m0}$)
$\frac{H_{m0,LF}}{H_{m0}} = 0.75kh^{-1.15}s_{m-1,0,deep}^{0.50}$	(17)	1/100,1/50 and 1/20	0.071
$\frac{H_{m0,LF}}{H_{m0}} = 0.85kh^{-1.18}s_{m-1,0,deep}^{0.53}$	(18)	1/100	0.070
$\frac{H_{m0,LF}}{H_{m0}} = 0.75kh^{-1.20}s_{m-1,0,deep}^{0.50}$	(19)	1/50	0.044
$\frac{H_{m0,LF}}{H_{m0}} = 0.66kh^{-1.11}s_{m-1,0,deep}^{0.49}$	(20)	1/20	0.030
$\frac{H_{m0,LF}}{H_{m0}} = 0.53kh^{-1.19}s_{m-1,0,deep}^{0.53}m^{0.1}$	(21)	1/100,1/50 and 1/20	0.060

a γ_f of 0.40 (as proposed for rock by EurOtop, 2018) for EurOtop (2018) and Van Gent et al. (2022) (Only shown in Table 6). The TAW formulation underestimated the wave overtopping discharge, especially for shallow water conditions (Figure Fig. 10(a)). The formulation of Koosheh et al. (2022) derived based on tests without wave breaking on the foreshore shows less scatter for the larger overtopping discharges, but a large deviation for the lower overtopping discharges. Due to this large deviation for lower overtopping discharges, the statistical scores are similar to the scores obtained with Eq. (3), although the results are better for the higher overtopping discharges. The better performance for the larger overtopping discharges can be explained by the addition of the wave steepness in the expression. The expression given in Van Gent et al. (2022) performs better, without the overestimation of the lower discharges, than Koosheh et al. (2022) with an RMSLE of 1.29 (Shown in Table 6). The results for Van Gent (1999) (Eq. (4)) show the best performance with a RMSLE of 1.10. This expression was derived for overtopping of dikes in shallow water conditions and is therefore most similar to the current dataset. When the formulation from the EurOtop (2018) is applied an RMSLE of 2.92 is found. The large scatter for the EurOtop (2018) expression is caused by the roughness formulation based on the wave steepness which deviates significantly in shallow water.

5.2. Determine important wave parameters

A large amount of scatter was found in the existing formulations, which were mostly derived for conditions without wave breaking on the foreshore when compared to the current dataset that includes conditions with wave breaking on the foreshore. To derive a new expression for conditions that include wave breaking on the foreshore, first, the importance of various wave parameters on the mean overtopping discharge is studied. A machine learning technique is applied to assess the importance of the different wave parameters on the mean wave overtopping. The non-dimensional mean overtopping discharge is predicted with a random forest regressor. A random forest regressor is a machine-learning technique that predicts a variable, in this case, the mean overtopping discharge, based on several input parameters with a large decision tree. For a complete description of this method see Breiman (2001) or Geurts et al. (2006). For four sets of input parameters, the random forest regressor is optimized to predict the non-dimensional mean overtopping discharge ($q^* = q/\sqrt{gH_{m0}^3}$). For each of the optimized models, the feature importance is determined, which indicates how important a parameter is for the prediction. The results of this analysis are shown in Table 5. In essence, these optimized models could also be applied to predict the mean overtopping discharge, but these models do not show the dependencies on the input parameters and the current dataset is too small to set up a robust model for the mean overtopping discharge. Therefore, it is only used to show the importance of several wave parameters.

Since the spectral shape changes significantly in extremely shallow water, the wave steepness becomes very low. The energy at the lower frequencies results in a very large spectral wave period, but this spectral period does not represent the steepness of the short waves anymore. Therefore, a new definition of the wave steepness is defined where only the high frequency part is considered ($H_{m0,HF}$ and $T_{m-1,0,HF}$). This short-wave steepness ($s_{m-1,0,HF}$) represents the actual wave steepness of the short waves.

This feature importance for various sets of input parameters shows that the most important parameter to predict mean overtopping discharge is the relative crest height (R_c/H_{m0}, with a feature importance of 0.51 for Nr 1). When all the dimensional parameters are included (Nr 1 in Table 5) the wave asymmetry (0.13) and relative water depth (0.13) are the second most important parameters, showing that the wave shape and local water depth are important parameters for the mean overtopping discharge in shallow water. However, wave asymmetry and wave skewness are not typical wave parameters that are easily accessible, both with numerical models and empirical formulations. When the model is optimized on a dataset without the asymmetry and skewness the importance of the remaining parameter changes (Nr 3). The short-wave steepness ($s_{m-1,0,HF}$) becomes the second most important parameter (feature importance of 0.15 in Nr 2) and the contribution of the relative water depth decreases. In the third optimization (Nr 3), the relative water depth is also removed as an input parameter. The contribution of the relative water depth is relatively large but it is argued that a formulation without the water depth is preferred. The reason is twofold. Firstly, the definition of the water depth is not trivial, especially for complex foreshores. Secondly, a formulation based on only wave conditions could also apply to other complex foreshores. For example, if there is a bar in front of the structure, the local water depth does not account for the bar whereas an expression based on the wave parameters includes the effect of the bar. The wave parameter at the location of the structure, determined with a numerical model, would include the effects of the bar. The same holds for the Iribarren number based on the foreshore slope ($\xi_{m-1,0,foreshore}$) which also has a relatively large contribution. Thus, when also the relative water depth (H_{m0}/h) and Iribarren number are removed (Nr 3 and Nr 4) from the input the importance of the short-wave steepness increases even more (0.18) and the contribution of the low-frequency wave height becomes more important (0.08). All the other parameters do not show a significant effect on the mean overtopping discharge. This does not necessarily mean that these parameters do not affect the mean overtopping discharge but their contribution could be described by another wave parameter (see Section 6). Thus, this analysis reveals that when the wave asymmetry, relative water depth and Iribarren number are not used because these parameters are not always characteristic of the wave conditions, the combination of the low-frequency wave height with the short-wave steepness is important.

5.3. Expression for the mean overtopping discharge

The feature importance analysis showed which parameters are important to predict the mean overtopping discharge. To quantify the mean overtopping discharge, several formulations are fitted. By adding complexity into the fitted formulations it is possible to show the effect of the added complexity. Besides the RMSLE computed over the entire

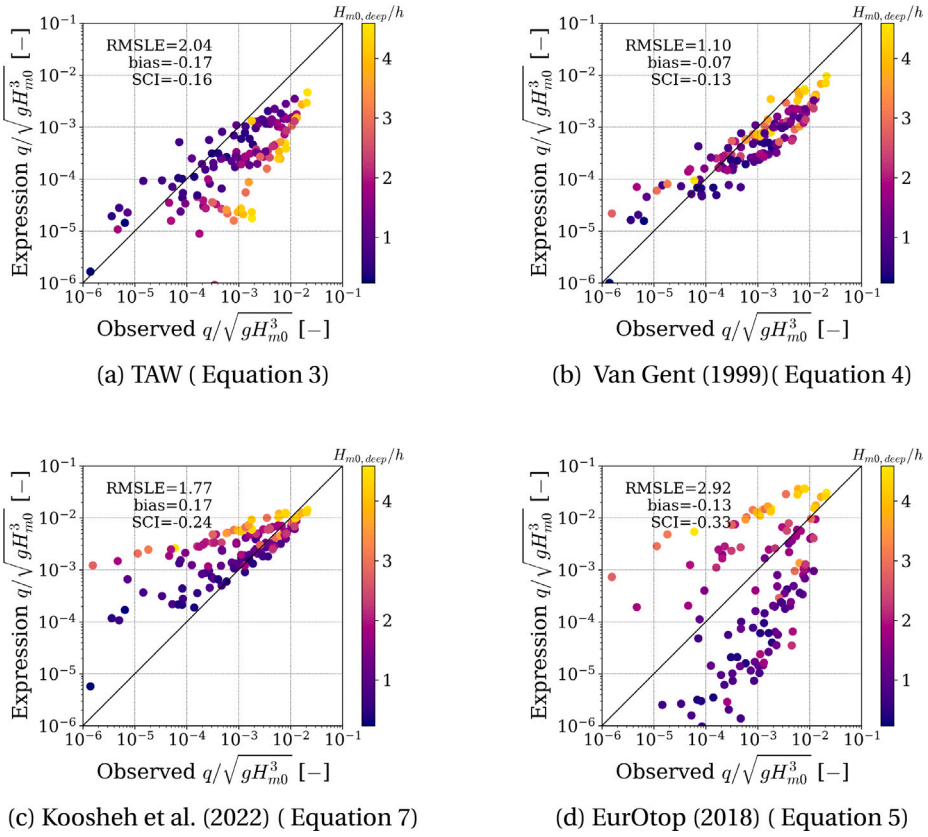

(a) TAW (Equation 3)

(b) Van Gent (1999)(Equation 4)

(c) Koosheh et al. (2022) (Equation 7)

(d) EurOtop (2018) (Equation 5)

Fig. 10. Scatter plot of mean wave overtopping for four different formulations. The relative water depth of each point is shown with the colour of the marker. The statistical scores are shown for the data points where $q^* > 10^{-6}$ ($N = 133$).

Table 5
Feature importance for a random forest regressor with different input wave parameters for predicting the non-dimensional mean overtopping discharge. Each column shows the feature importance and the RMSLE for a fit with the random forest regressor, with the applied parameters changing in each column.

Optimization Nr	1	2	3	4
R_c/H_{m0}	0.51	0.51	0.53	0.55
H_{m0}/h	0.13	0.12	–	–
A_s	0.13	–	–	–
S_k	0.02	–	–	–
$s_{m-1,0,HF}$	0.06	0.15	0.18	0.22
$s_{m-1,0}$	0.01	0.03	0.03	0.04
$\xi_{m-1,0,foreshore}$	0.05	0.07	0.11	–
$H_{m0,LF}/H_{m0}$	0.03	0.05	0.08	0.08
$H_{2\%}/H_{m0}$	0.02	0.04	0.04	0.04
$\langle\eta\rangle/H_{m0}$	0.02	0.04	0.04	0.06
RMSLE ($q/\sqrt{gH_{m0}^3}$)	0.316	0.346	0.363	0.362

dataset, the RMSLE is also shown for parts of the dataset in Table 6. The typical exponential wave overtopping formulation is used as the basis of the expression. Moreover, the relation between the non-dimensional overtopping discharge and various options for the non-dimensional crest height is shown in Fig. 11. The roughness factor (γ_f) is set to 0.55 as given by TAW (2002).

When only the relative crest height is considered in the formulations the RMSLE is relatively large (1.34). By adding the wave steepness in the formulation the fit improves significantly (1.34 to 0.79). A further improvement is found when the wave steepness is based on the high-frequency part of the spectrum ($s_{m-1,0,HF}$). This means that the wave period of the short waves is important to predict the mean wave overtopping discharge. Especially, in extremely shallow water the wave steepness defined on the entire frequency range is mainly dominated by the low-frequency energy, whereas the period of the short waves contributes to the overtopping volume. To include the low-frequency wave height in the expression it is chosen to include this wave height in the relative crest height as a reduction of the crest height as proposed by Van Gent (2021, 2022). When the low-frequency wave height is added to the expression the accuracy further increases. Note that the improvement found when adding the low-frequency wave height does not represent the importance of the low-frequency wave height for overtopping because the short-wave steepness implicitly includes the effects of the low-frequency wave height. The low-frequency wave height and the short-wave steepness are correlated. When including the low-frequency wave height, the results become more accurate when the mean overtopping discharge is normalized with the short-wave height (see Eq. (26) and Eq. (27)).

Next to the inclusion of the low-frequency wave height, the relative crest height is expressed in terms of the 2% exceedance wave height. As shown in Fig. 5 the 2% exceedance wave height captures both the effect of wave breaking and the low-frequency wave height. By adding only the 2% exceedance wave height the accuracy decreases, but when the low-frequency wave height is included in the relative crest height the accuracy increases. Apparently, the combination of both parameters is required to accurately predict the mean overtopping discharge.

When considering the uncertainty related to the low-frequency wave height and 2% exceedance wave height (see Figs. 9 and 5), Eq. (24) could be desired in practical applications. The improvement in terms of mean overtopping discharge is not significant compared to the uncertainty of the wave parameters when determined with empirical formulations or most of the numerical models. The effect of noise on the input parameter is demonstrated in Section 6 where it is shown

Table 6
Overview of RMSLE for various equations and subsets of the datasets. The number of data points is 133. Deep is defined as $H_{m0,deep}/h < 0.4$ (7 points), Intermediate defined as $0.4 < H_{m0,deep}/h < 1$ (33 points) and shallow is defined as $H_{m0,deep}/h > 1$ (93).

Formulation		RMSLE $(q/\sqrt{gH_{m0}^3})$ [–]			
		All	Deep	Inter- mediate	Shallow
Eq. (3) (TAW, 2002)		2.04	0.71	1.05	2.35
Eq. (4) (Van Gent, 1999)		1.10	0.86	1.08	1.13
Eq. (5) (EurOtop, 2018)		2.92	4.32	3.34	2.62
Eq. (7) (Koosheh et al., 2022)		1.77	1.47	1.61	1.85
Eq. (8) (Van Gent et al., 2022)		1.29	1.43	1.14	1.33
$\frac{q}{\sqrt{gH_{m0}^3}} = 0.25\exp\left(-2.12\frac{R_c}{H_{m0}\gamma_f}\right)$	(22)	1.34	1.86	1.68	1.15
$\frac{q}{\sqrt{gH_{m0}^3}} = 1.27\exp\left(-5.05\frac{R_c}{H_{m0}\gamma_f}s_{m-1,0}^{0.12}\right)$	(23)	0.79	0.87	0.93	0.73
$\frac{q}{\sqrt{gH_{m0}^3}} = 0.74\exp\left(-8.51\frac{R_c}{H_{m0}\gamma_f}s_{m-1,0,HF}^{0.32}\right)$	(24)	0.69	1.05	0.82	0.60
$\frac{q}{\sqrt{gH_{m0}^3}} = 0.54\exp\left(-11.33\frac{R_c}{H_{2\%\gamma_f}}s_{m-1,0,HF}^{0.34}\right)$	(25)	0.77	1.29	0.82	0.70
$\frac{q}{\sqrt{gH_{m0}^3}} = 0.50\exp\left(-7.91\frac{R_c - 0.21H_{m0,LF}}{H_{m0}\gamma_f}s_{m-1,0,HF}^{0.30}\right)$	(26)	0.68	0.98	0.82	0.60
$\frac{q}{\sqrt{gH_{m0,HF}^3}} = 0.44\exp\left(-8.75\frac{R_c - 0.38H_{m0,LF}}{H_{m0}\gamma_f}s_{m-1,0,HF}^{0.33}\right)$	(27)	0.67	1.04	0.79	0.58
$\frac{q}{\sqrt{gH_{m0,HF}^3}} = 0.15\exp\left(-9.45\frac{R_c - 0.90H_{m0,LF}}{H_{2\%}\gamma_f}s_{m-1,0,HF}^{0.28}\right)$	(28)	0.64	0.71	0.74	0.59

that an error of 10% can already result in a significant increase of the RMSLE.

It is verified whether the wave steepness should be included in the exponential or outside the exponential, but the best results were obtained when the wave steepness is included in the exponential. In a similar way as the low-frequency wave height, the effect of the setup is included in the exponent. However, these results were less accurate than the present formulations in Table 6.

The statistic scores are also shown for various subsets of the entire dataset. When the order of the accuracy deviates much between the different subsets it could indicate overfitting. Only for the deep water conditions, the order of the formulations based on the accuracy changes significantly but this subset also does not have many data points. Considering the existing formulations, it can also be seen that Eq. (3) show the best results for the deep water conditions ($H_{m0,deep}/h < 0.4$) and Eq. (4) performs better in shallow water conditions. Eq. (8) also performs reasonable accurate in shallow water.

5.4. Effect of foreshore slope and relative water depth on non-dimensional mean overtopping discharge

For Eq. (24) the scatter plots of the non-dimensional mean overtopping discharges are shown in Fig. 12. Eq. (24) is not the expression with the highest accuracy, but the most promising expression in terms of typical application. In Panel A of Fig. 12 the colours of the points indicate the foreshore slope. This figure shows that the foreshore slope is not causing the existing scatter after the fit. It can only be observed that in general, the 1:20 slope tests resulted in larger overtopping discharges than the tests with a 1:100 and 1:50 foreshore slope. The same holds for the relative water depth (Panel B of Fig. 12). Also, the relative water depth does not explain the scatter between the observation and the expression. Thus, by only including the wave height and short-wave steepness it is possible to describe the wave overtopping in shallow water while the effects of the foreshore slope and water depth can be captured with the wave conditions.

Table 7
RMSLE for variations in the f_{cutoff} between the short and long waves for formulation 3 and 6 from Table 6.

f_{cutoff}	Eq. (24): RMSLE $q/\sqrt{gH_{m0}^3}$ (–)	Eq. (27): RMSLE $q\sqrt{gH_{m0}^3}$ (–)
$f_p/1.1$	0.61	0.59
$f_p/1.25$	0.60	0.55
$f_p/1.5$	0.59	0.55
$f_p/1.75$	0.59	0.55
$f_p/2$	0.59	0.56
$f_p/2.25$	0.59	0.56

5.5. Sensitivity to cutoff frequency

To determine the cutoff frequency between the short and long waves, the performance of the fit for the mean overtopping discharge is evaluated for various cutoff frequencies. Especially in shallow water, this cutoff frequency will have a large effect on the energy of low-frequency waves and to a lesser extent on the short-wave steepness. For example in Fig. 7, it can be observed that most of the energy is present at the lower frequencies making the low-frequency wave height very sensitive to the cutoff frequency. To verify this sensitivity, multiple cutoff thresholds are verified in Table 7. When Eq. (24) is used, the best results are obtained with a cutoff frequency larger than $f_p/1.25$. For Eq. (28) the best results are obtained for a cutoff frequency between $f_p/1.25$ and $f_p/1.75$. Therefore a cutoff frequency of $f_p/1.5$ is applied in this study. In this study, a cutoff frequency based on the peak period is possible because the offshore spectrum is given by a smooth JONSWAP spectral shape, but for practical application, this definition is not suitable because the peak frequency is not always easy to determine. In order to accurately determine the cutoff frequency for practical applications, the optimal cutoff frequency is rewritten in terms of the spectral period ($T_{m-1,0}$) by assuming a JONSWAP spectral shape. Given the relation between the T_p and the $T_{m-1,0}$ of 1.1 for a JONSWAP spectrum, the recommended cutoff frequency for practical applications becomes $f_{cutoff} = 0.45/T_{m-1,0}$.

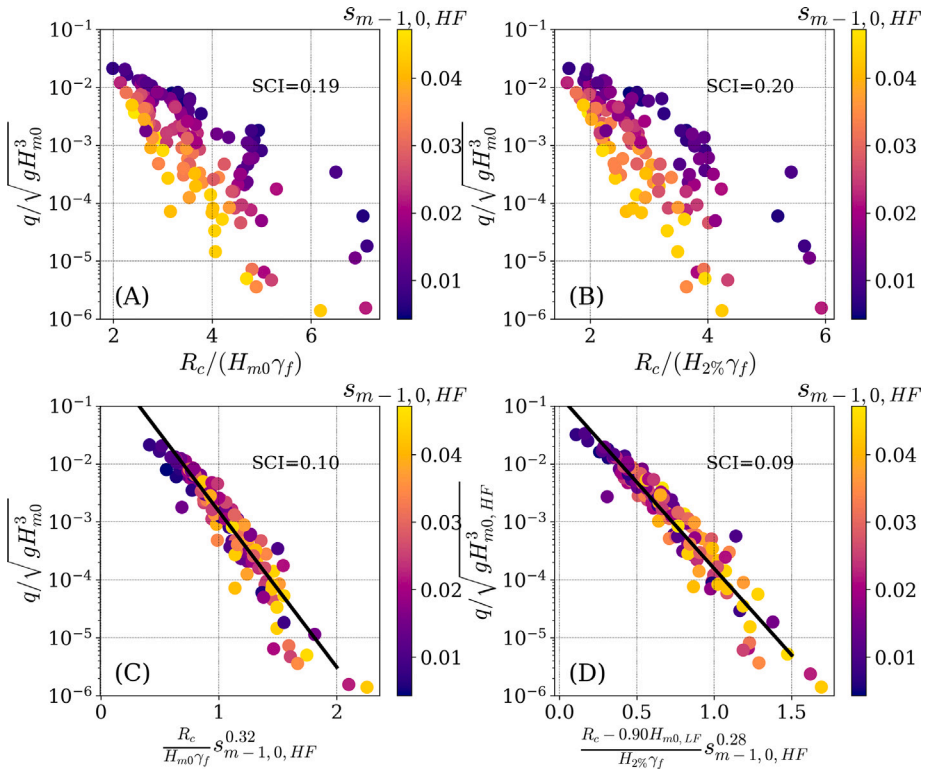

Fig. 11. Mean wave overtopping discharge as a function of four different relative crest levels. The colours in each panel represent the short-wave steepness. Panel C shows the scatter of Eq. (24) and Panel D shows the scatter of Eq. (28). The SCI of the linear fit between the variables on the x-axis and the logarithmic of the non-dimensional wave overtopping (y-axis) is shown in each panel.

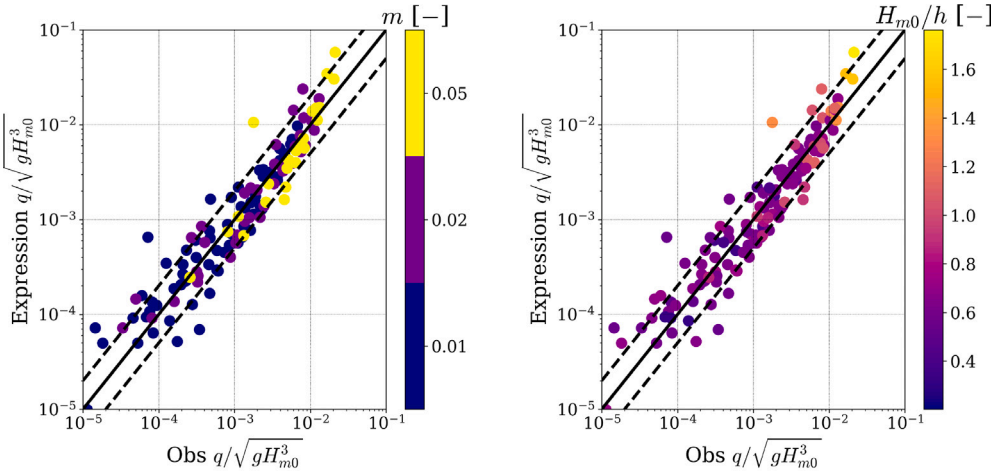

Fig. 12. Scatter plot of non-dimensional mean overtopping discharges between the observation (x-axis) and the model (y-axis). Next to the scatter, the 1:1 line and factor two lines (x 2, x 0.5) are shown in black. The left panel shows the scatter with the colours indicating the foreshore slope and the right panel shows the scatter with the colours indicating the relative water depth (H_{m0}/h).

6. Discussion

In this study, the obtained formulations for the mean overtopping discharge are evaluated with the measured data, but in reality, the wave conditions at the location of the structure are not available and need to be predicted with empirical formulations or numerical models. As a consequence, the input wave parameters for the formulation will also contain uncertainty. To show how this uncertainty in the wave parameters affects the prediction of the non-dimensional mean overtopping discharge, the non-dimensional overtopping mean discharge

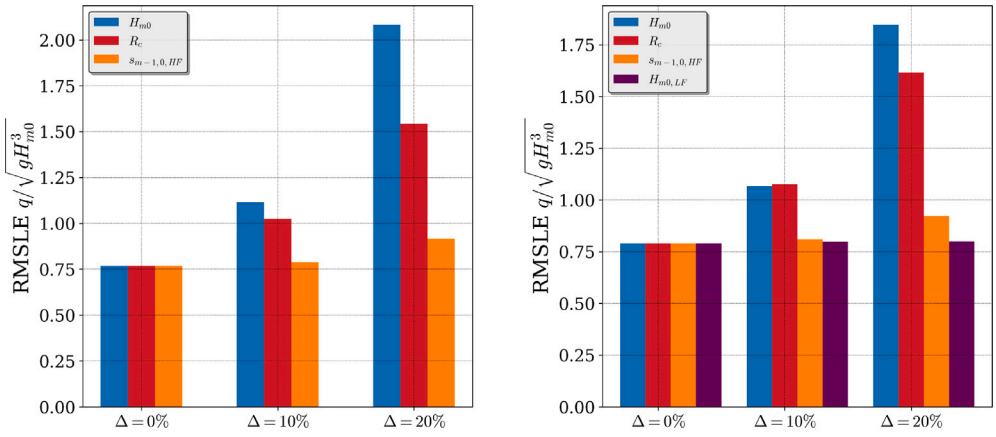

(a) Equation 24 (b) Equation 27

Fig. 13. Bar plot with the RMSLE of the non-dimensional mean overtopping discharge ($q/\sqrt{gH_{m0}^3}$) for Eq. (24) and Eq. (27) with noise added to the input parameters.

is computed with Eq. (24) and Eq. (27) for the same dataset but with noises added to respectively the wave height, crest height, short-wave steepness and low-frequency wave height (Fig. 13). When adding (Gaussian) noise with an amplitude of 10% and 20% it can be observed that the wave height is the most sensitive parameter for predicting the non-dimensional mean overtopping discharge. When 10% noise is added to the wave height, the RMSLE increases up to almost 2. For the crest height and wave steepness, this is lower with the wave steepness having the least influence. This high influence of the wave height can be explained by the fact that the wave height is both included in the relative crest and in the non-dimensional overtopping discharge. Considering Eq. (27) the low-frequency wave height is not very sensitive to noise. Only Eq. (24) and Eq. (27) were verified to get an indication of the uncertainty for a formulation with the wave height, crest level and short-wave steepness (Eq. (24)) and a formulation which also includes the low-frequency wave height (Eq. (27)).

Thus when the input wave condition contains an uncertainty larger than 10% it does not make sense to apply Eq. (25), Eq. (27) or Eq. (28) instead of Eq. (24), because the uncertainty in the input wave conditions is significantly larger than the error reduction caused by a more advanced formulation. Moreover, this analysis demonstrates that it is important to accurately model the nearshore wave parameters.

The effect of various wave parameters on the mean overtopping discharge is studied. It appears that the short-wave steepness and relative crest height are the most important wave parameters, although it is observed that for example the wave setup and low-frequency wave height become significant in shallow water (see Figs. 9 and 6) and will also affect the wave overtopping. A reason why these wave parameters do not have a large contribution to the accuracy when included in the formulation is because the various wave parameters are correlated. The short-wave steepness captures the following physical processes:

- Wave breaking: In general low short-wave steepness conditions will result in a higher mean overtopping discharge because these wave conditions tend to have less wave breaking.
- Low-frequency waves: The short-wave steepness is correlated to the low-frequency wave height in shallow water. Wave conditions with a long wave period, will result in more energy transfer to the lower frequencies (e.g. Longuet-Higgins and Stewart, 1964). Thus, a low short-wave steepness condition in shallow water will have significant energy at the lower frequencies resulting in a larger mean overtopping discharge.

The total wave steepness cannot be applied in shallow water because it is dominated by the energy at the lower frequencies making it less representative of the wave field. Similar to the effect of the low-frequency wave height, also the effect of the wave setup is indirectly captured with the other wave parameters (wave height, short-wave steepness and low-frequency wave height). By adding the 2% exceedance wave height the effect of the shape of the wave height exceedance distribution is included in the formulation caused by wave breaking but this parameter is also highly related to the low-frequency wave height in shallow water (see Fig. 5).

Due to these correlations, it is therefore difficult to capture, for example, purely the effects of low-frequency waves next to the effects of the wave steepness in an empirical formulation. It is therefore recommended to verify the existing expression for a dataset with more data points where the correlation between the wave parameters is lower.

The current findings are valid for long-crested waves without directional spreading. The energy transfer to the longer wave periods is less pronounced in short-crested sea states (Klopman and Dingemans, 2001, e.g.). This will affect the wave overtopping because fewer waves can reach the structure when the energy of the low-frequency waves is lower. When the effect of the low-frequency waves on wave overtopping is included in the overtopping formulation, the current findings would also be valid for short-crested sea states. For the same wave condition, the low-frequency wave height is only lower in a short-crested sea state but this effect would be accounted for in the overtopping formulation. However, it is observed that the effect of the low-frequency waves is also present in other wave parameters. For example, the short-wave steepness is correlated to the low-frequency wave height and the total wave height is also related to the low-frequency wave height. Thus it is recommended to also study the effects of shallow water for short-crested sea states because it is possible that there are correlations between wave parameters in the current dataset which do not occur in a dataset with short-crested wave conditions.

In the current analysis, the roughness and the structure geometry are not considered whereas it is known that these factors also play a role in describing the wave overtopping (see latest developments in Chen et al., 2020; Van Gent et al., 2022). Since the structure geometry and the roughness are not changed in the experiments the effects of these processes are included in the derived coefficients. The roughness effects are typically given with a roughness factor in the relative crest height and could easily be included by dividing the coefficients with the roughness factor. The same holds for the structure slope. To be able to apply the expression for different structure geometries and roughness, it is recommended to verify the current findings for structures with a different geometry (e.g. slope, roughness and permeability).

The formulations in Table 6 show that including the short wave steepness improves the accuracy of the overtopping formulation compared to the formulation with the wave steepness based on the entire

frequency range. However, the short wave steepness is not a wave parameter commonly applied in coastal engineering. But it is argued that this is not a large limitation for applying, for example, Eq. (24) because one needs to apply a numerical model to obtain the nearshore wave conditions at the toe of the structure for shallow water conditions and most numerical models provide the wave spectrum from which the short wave steepness can be obtained.

7. Conclusions

Wave overtopping has been studied using physical model experiments with rubble mound breakwaters in shallow water with severe wave breaking. The mean overtopping discharge is determined for three different foreshore slopes and various hydrodynamic conditions.

The shallow foreshore causes that wave energy is transferred from frequencies around the peak of the short waves to low-frequency waves resulting in conditions where up to 70% of the energy is given by low-frequency waves. The results also show that in relatively deep water, the low-frequency wave is out of phase with the short waves, but is in phase with the short waves in very shallow water as also found by several other authors. However, in this study, the effect of this correlation between the short waves and the low-frequency wave in very shallow water on the higher short waves (e.g. the 2% exceedance wave height), important for wave overtopping, is shown. These higher waves become relatively large in extremely shallow water. The ratio between the 2% exceedance wave height and the short-wave height at the toe of the structure becomes larger than in deep water (about 1.4).

To estimate the amount of energy at the low-frequency waves, an expression is derived to predict the fraction of low-frequency waves based on the local water depth, wave number of the deep water spectral period, deep water wave steepness and foreshore slope (Eq. (21)). This expression shows reasonably good results with an RMSE of 0.06 for the fraction of low-frequency waves.

When considering the non-dimensional mean wave overtopping discharge the existing formulations perform poorly to reasonably in shallow water with RMSLE ranging from 1.04 to 2.92. A parameter sensitivity study shows that the short-wave steepness, relative crest height and low-frequency wave height mostly affect the mean overtopping discharge. When including the short-wave steepness and relative crest height in an empirical formulation the RMSLE for the current dataset reduces to 0.69 (Eq. (24)). To further improve the formulation the low-frequency wave height and 2% exceedance wave height are required resulting in an RMSLE of 0.64 (Eq. (27)).

All these results are obtained for straight foreshores (1:20. 1:50 and 1:100) and it is recommended to verify the formulation for more complex foreshores. Moreover, the current findings are based on tests with long-crested waves and the results should be verified for short-crested waves. In addition, it is recommended to also study the individual volumes for a structure in shallow water.

CRediT authorship contribution statement

Menno P. de Ridder: Writing – original draft, Visualization, Formal analysis. **Dennis C.P. van Kester:** Writing – review & editing, Supervision. **Rick van Bentem:** Writing – review & editing, Supervision. **Djimin Y.Y. Teng:** Writing – review & editing, Formal analysis. **Marcel R.A. van Gent:** Writing – review & editing, Supervision, Project administration, Conceptualization.

Declaration of competing interest

The authors declare that they have no known competing financial interests or personal relationships that could have appeared to influence the work reported in this paper.

Data availability

The data that has been used is confidential.

Acknowledgements

This study was realized with the help of a TKI (Top Consortia for Knowledge and Innovation) subsidy (Delta Technology project CLIMACS, project DEL171) and the support by the 'Vereniging van Waterbouwers'. The assistance by our colleague Mr. Wesley Stet during the actual model testing is highly appreciated.

Appendix A. Incident waves

In Fig. A.14 the effects of the two methods to obtain the incident waves are shown. The top panel shows a scatter plot between the parameters measured before the structure (tests with the structure in place) and those obtained at the toe of the structure during the calibration test conducted in the absence of the structure. Both results show the incident wave parameters decomposed with the decomposition method described in De Ridder et al. (2023). This result shows that the location where the wave parameters are measured is very relevant in shallow water. Due to wave breaking, the wave height is significantly lower at the toe of the structure compared to the location before the structure. On the other hand, the spectral period is much longer at the toe of the structure compared to the location before the structure. This is explained by the fact short waves break and energy is transferred to the longer waves making the spectral period longer. The last column shows how the location influences the non-dimensional mean overtopping discharge.

The lower panels show a similar comparison but now with two decomposition approaches (V1 and V2). Approach V1 is the incident wave as obtained from the method described in De Ridder et al. (2023). In Approach 2 the measured short-wave signal is assumed to be equal to the incident wave signal and only the decomposition for the low frequency range is performed. This effect shows the wave height and 2% exceedance wave height is slightly higher when Approach V2 is applied. This is caused by the fact that some of the conditions are very nonlinear making the decomposition not applicable. The trend for the spectral period is different. Energy at the higher frequencies is missing with the decomposition method resulting in an overestimation of the spectral period when the decomposition is applied.

This analysis shows that the location and the decomposition method can have a large effect on the results when considering shallow water conditions.

Appendix B. Cross-correlation function

The cross-correlation function ($R_{\eta_{LF}(t)A(t+\tau)}$) as function of a time shift (τ) for several wave gauge is shown in Fig. B.15 for Test A911 (1:100 foreshore, $H_{m0}/h = 2$, $s_{m-1,0} = 0.01$). The maximum correlation (both positive and negative) is shown with a red dot. In relatively deep water the maximum correlation is negative with a time shift of approximately 0. When the water depth decreases, the time shift becomes longer showing that the low-frequency wave lags behind the short-wave group. When the water depth is very shallow and the low-frequency wave is free, the correlation becomes positive. The short-wave group is in phase with the low-frequency wave. also for these extremely shallow water depths, a time shift is visible showing that the short waves lag behind the low-frequency wave.

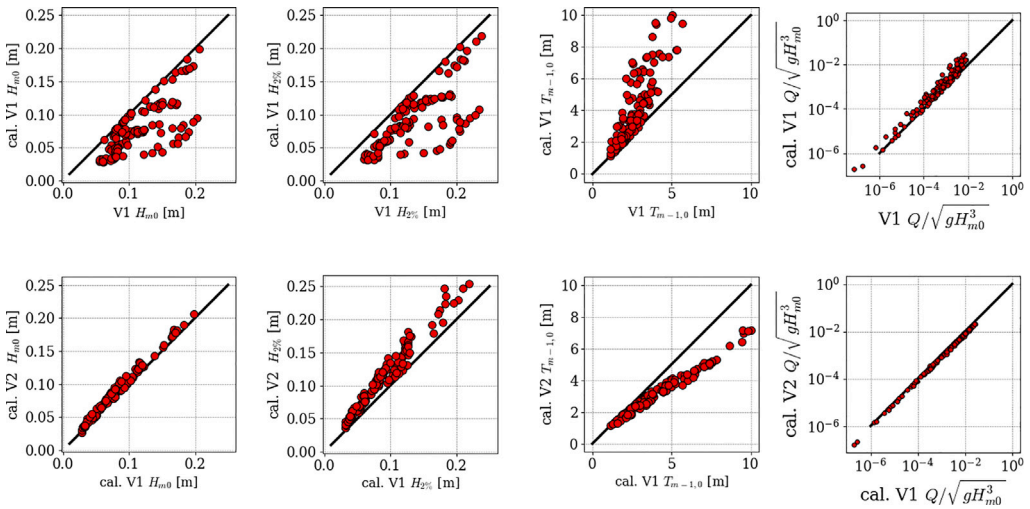

Fig. A.14. Scatter plot of the Wave height, 2% exceedance wave height, spectral period and non-dimensional mean overtopping discharge. The top panels show the comparison between (x-axis) incident wave parameter before the structure and (y-axis) wave parameter at the location of the structure during the calibration test. The lower panels show the comparison between (x-axis) incident wave parameter at the location of the structure during the calibration test analysed with Approach V1 and (y-axis) wave parameter at the location of the structure during the calibration test analysed with Approach V2. The wave parameters are obtained from Set two.

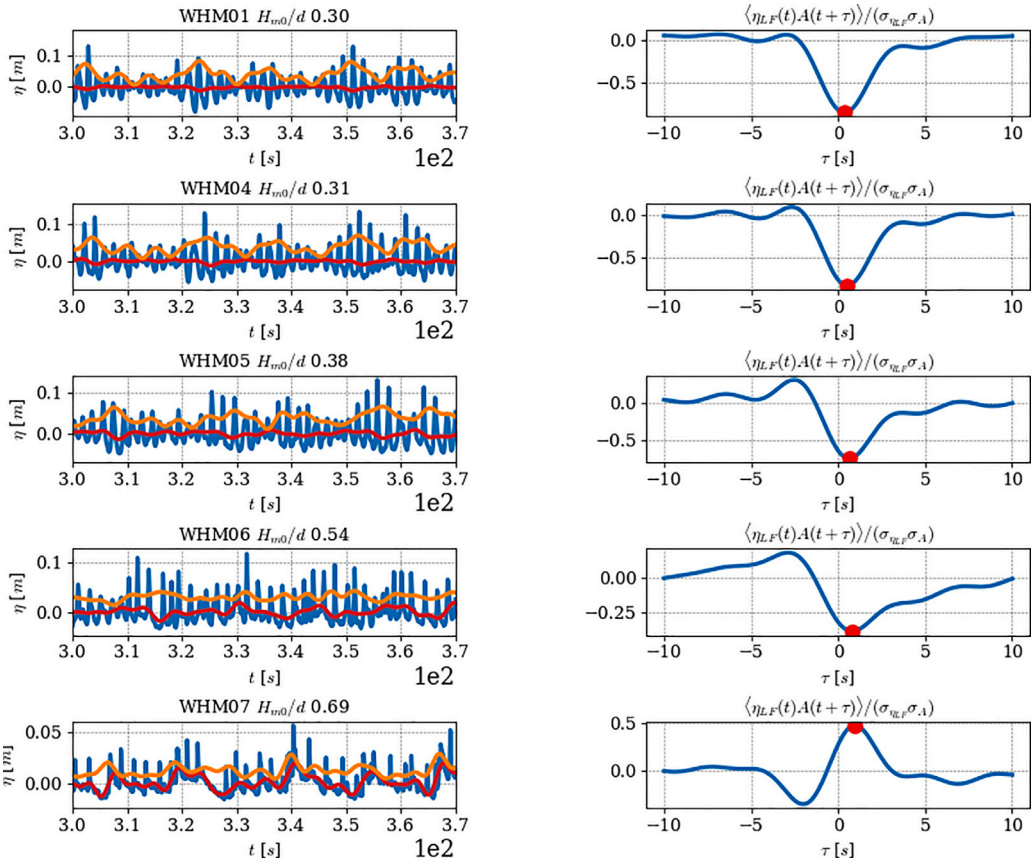

Fig. B.15. Time series of low-frequency signal (red), short-wave group (orange) and measured signal (blue) shown on the left panels. The right panels show the cross-correlation function as a function of a time shift (τ). The maximum (positive or negative) correlation is shown with a red dot. The vertical panels show the result for various wave gauges.

References

Altomare, C., Suzuki, T., Chen, X., Verwaest, T., Kortenhaus, A., 2016. Wave overtopping of sea dikes with very shallow foreshores. Coast. Eng. 116, 236–257.

Battjes, J.A., 1972. Golfoploop en golfoverslag.

Battjes, J.A., 1974. Computation of set-up, longshore currents, run-up and overtopping due to wind-generated waves (Ph.D. thesis).

Battjes, J.A., Bakkenes, H.J., Janssen, T.T., van Dongeren, A.R., 2004. Shoaling of subharmonic gravity waves. J. Geophys. Res.: Oceans 109 (C2).

Battjes, J.A., Groenendijk, H.W., 2000. Wave height distributions on shallow foreshores. Coast. Eng. 40 (3), 161–182.

Breiman, L., 2001. Random forests. Mach. Learn. 45, 5–32.

Chen, W., Marconi, A., Van Gent, M.R.A., Warmink, J.J., Hulscher, S.J.M.H., 2020. Experimental study on the influence of berms and roughness on wave overtopping at rock-armoured dikes. J. Mar. Sci. Eng. 8 (6), 446.

De Ridder, M.P., Kramer, J., den Bieman, J.P., Wenneker, I., 2023. Validation and practical application of nonlinear wave decomposition methods for irregular waves. Coast. Eng. 183, 104311.

De Waal, J.P., Van der Meer, J.W., 1993. Wave runup and overtopping on coastal structures. In: Coastal Engineering 1992. pp. 1758–1771.
Eldrup, M.R., Lykke Andersen, T., 2024. Generation of highly nonlinear waves in a short wave flume. CoastLab 2024 Phys. Model. Coast. Eng. Sci..
EurOtop, 2007. EurOtop, European overtopping manual-wave overtopping of sea defences and related structures: assessment manual.
EurOtop, 2018. Manual on wave overtopping of sea defences and related structures.
Franco, L., De Gerloni, M., Van der Meer, J.W., 1995. Wave overtopping on vertical and composite breakwaters. In: Coastal Engineering 1994. pp. 1030–1045.
Geurts, P., Ernst, D., Wehenkel, L., 2006. Extremely randomized trees. Mach. Learn. 63, 3–42.
Goda, Y., Kishara, Y., Kamiyama, Y., 1975. Laboratory investigation on the overtopping rate of seawalls by irregular waves. In: Report of the Port and Harbour Research Institute. vol. 14, (4), PARI.
Hasselmann, K., 1962. On the non-linear energy transfer in a gravity-wave spectrum part 1. general theory. J. Fluid Mech. 12 (4), 481–500.
Hedges, T.S., Reis, M.T., Owen, M.W., 1998. Random wave overtopping of simple sea walls: A new regression model.. Proc. Inst. Civ. Eng. Water Marit Energy 130 (1), 1–10.
Janssen, T.T., Battjes, J.A., Van Dongeren, A.R., 2003. Long waves induced by short-wave groups over a sloping bottom. J. Geophys. Res.: Oceans 108 (C8).
Kikkawa, H., Shi-igai, H., Kono, T., 1968. Fundamental study of wave over-topping on levees. Coast Eng. Japan 11 (1), 107–115.
Klopman, G., Dingemans, M.W., 2001. Wave interactions in the coastal zone. Proc. 16th Int. Workshop Water Waves and Float. Bodies.
Koosheh, A., Etemad-Shahidi, A., Cartwright, N., Tomlinson, R., Van Gent, M.R.A., 2022. Experimental study of wave overtopping at rubble mound seawalls. Coast. Eng. 172, 104062.
Lashley, C.H., Van der Meer, J., Bricker, J.D., Altomare, C., Suzuki, T., Hirayama, K., 2021. Formulating wave overtopping at vertical and sloping structures with shallow foreshores using deep-water wave characteristics. J. Waterw. Port Coastal Ocean. Eng. 147 (6), 04021036.
Longuet-Higgins, M.S., Stewart, R.W., 1962. Radiation stress and mass transport in gravity waves, with application to 'surf beats'. J. Fluid Mech. 13 (4), 481–504.
Longuet-Higgins, M.S., Stewart, R., 1964. Radiation stresses in water waves; a physical discussion, with applications. In: Deep Sea Research and Oceanographic Abstracts. 11, (4), Elsevier, pp. 529–562.
Van der Meer, J.W., Janssen, J.P.F.M., 1994. Wave run-up and wave overtopping at dikes and revetments. Delft Hydraulics, publication no. 485.
Owen, M.W., 1980. Design of seawalls allowing for wave overtopping, HR-wallingford. Technical Report, UK, Technical Report EX-924.
Saville, T., 1955. Laboratory Data on Wave Run-Up and Overtopping on Shore Structures. (64), US Beach Erosion Board.
Suedel, B.C., Calabria, J., Bilskie, M.V., Byers, J.E., Broich, K., McKay, S.K., Tritinger, A.S., Woodson, C.B., Dolatowski, E., 2022. Engineering coastal structures to centrally embrace biodiversity. J. Environ. Manag. 323, 116138. http://dx.doi.org/10.1016/j.jenvman.2022.116138, URL https://www.sciencedirect.com/science/article/pii/S030147972201711X.
TAW, 2002. Wave Run-Up and Wave Overtopping at Dikes. Technical Report.
Van Gent, M.R.A., 1999. Physical model investigations on coastal structures with shallow foreshores: 2D model tests with single and double-peaked wave energy spectra.
Van Gent, M.R.A., 2001. Wave runup on dikes with shallow foreshores. J. Waterw Port Coast. Ocean. Eng. 127 (5), 254–262.
Van Gent, M.R.A., 2014. Oblique wave attack on rubble mound breakwaters. Coast. Eng. 88, 43–54.
Van Gent, M.R.A., 2019. Climate adaptation of coastal structures. In: Proceedings of the SCACR19—9th Short Course/Conference on Applied Coastal Research, Bari, Italy. pp. 9–11.
Van Gent, M.R.A., 2021. Influence of oblique wave attack on wave overtopping at caisson breakwaters with sea and swell conditions. Coast. Eng. 164, 103834.
Van Gent, M.R.A., 2022. Wave overtopping at dikes and breakwaters under oblique wave attack. Coast. Eng. Proc. (37), 5.
Van Gent, M.R.A., Giarrusso, C.C., 2005. Influence of foreshore mobility on wave boundary conditions. In: Proceedings of the International Conference on Ocean Waves Measurements and Analysis, Madrid, Spain. pp. 3–7.
Van Gent, M.R.A., Teng, D.Y.Y., 2023. Climate adaptation of coastal structures: Application of adaptation pathways for rubble mound breakwaters. Proc. PIANC-COPEDEC X, Manila.
Van Gent, M.R.A., Wolters, G., Capel, A., 2022. Wave overtopping discharges at rubble mound breakwaters including effects of a crest wall and a berm. Coast. Eng. 176, 104151.
Vuik, V., Jonkman, S.N., Borsje, B.W., Suzuki, T., 2016. Nature-based flood protection: The efficiency of vegetated foreshores for reducing wave loads on coastal dikes. Coast. Eng. 116, 42–56. http://dx.doi.org/10.1016/j.coastaleng.2016.06.001, URL https://www.sciencedirect.com/science/article/pii/S0378383916301004.